

Towards Analog Memristive Controllers

Gourav Saha, Ramkrishna Pasumarthy, and Prathamesh Khatavkar

Abstract—Memristors, initially introduced in the 1970s, have received increased attention upon successful synthesis in 2008. Considerable work has been done on its modeling and applications in specific areas, however, very little is known on the potential of memristors for control applications. Being nanoscopic variable resistors, one can consider its use in making variable gain amplifiers which in turn can implement gain scheduled control algorithms. The main contribution of this paper is the development of a *generic* memristive analog gain control framework and theoretic foundation of a gain scheduled robust-adaptive control strategy which can be implemented using this framework. Analog memristive controllers may find applications in control of large array of miniaturized devices where robust and adaptive control is needed due to parameter uncertainty and ageing issues.

Index Terms—BMI Optimization, Control of Miniaturized Devices, Gain Scheduling, Memristor, Robust and Adaptive Control

I. INTRODUCTION

MEMRISTOR [1], considered as the fourth basic circuit element, remained dormant for four decades until the accidental discovery of memristance in nanoscopic crossbar arrays by a group of HP researchers [2]. Memristor, an acronym for memory-resistor, has the capability of memorizing its history even after it is powered off. This property makes it a desirable candidate for designing high density non-volatile memory [3]. However, optimal design of such hardware architectures will require accurate knowledge of the nonlinear memristor dynamics. Hence, considerable effort has been channeled to mathematically model memristor dynamics (see [2], [4], [5], [6]). The memorizing ability of memristor has lead researchers to think about its possible use in neuromorphic engineering. Memristors can be used to make dense neural synapses [7] which may find applications in neural networks [8], character recognition [9], emulating evolutionary learning (like that of Amoeba [10]). Other interesting application of memristor may include its use in generating higher frequency harmonics which can be used in nonlinear optics [11] and its use in making programmable analog circuits [12], [13].

Memristor is slowly attracting the attention of the control community. Two broad areas have received attention: **1)** Control of Memristive Systems. This include works reported in [14], [15] give detailed insight into modelling and control of memristive systems in Port-Hamiltonian framework while State-of-the-Art work may include [16] which studies global stability of Memristive Neural Networks. **2)** Control using Memristive Systems. The very first work in this genre was reported in [17] where the author derived the describing function of a memristor which can be used to study the existence

The authors are with the Department of Electrical Engineering, Indian Institute of Technology, Madras, India. e-mail: {ee13s005, ramkrishna, ee13s007}@ee.iitm.ac.in

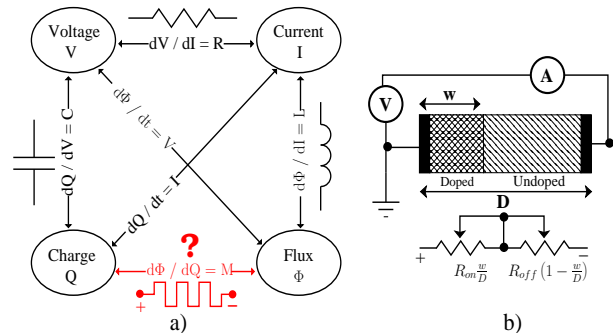


Figure 1. a) Memristor as a missing link of Electromagnetic Theory. Adapted from [4]. b) Memristor as a series resistor formed by doped and undoped regions of TiO_2 . Adapted from [2].

of undesirable limit cycles (i.e. sustained oscillations) in a closed loop system consisting of memristive controller and linear plant. Another line of work may include [18], [19] which uses memristor as a passive element to inject variable damping thus ensuring better transient response. In this paper we lay the groundwork to use memristor as an analog gain control (AGC) element for robust-adaptive control of miniaturized systems.

Why "Analog Memristive Controller"?: Several applications needs controlling an array of miniaturized devices. Such devices demands Robust-Adaptive Control due to parameter uncertainty (caused by design errors) and time varying nature (caused by ageing effect). Robust-Adaptive Control algorithms found in literature are so complex that they require microcontroller for implementation. This poses scalability and integration issues [20] (page 190) because microcontroller in itself is a complicated device. The motive of this work is two folded: 1) Invoke a thought provoking question: "Can modern control laws (like Robust-Adaptive control) be implemented using analog circuits¹?". 2) Suggest memristor as an AGC element² for implementing Robust-Adaptive Control.

The paper is organized as follows. We begin our study by gaining basic understanding of memristor in Section II. A generic gain control architecture using memristor is proposed in Section III. Section IV discusses a robust-adaptive control strategy which can be implemented in an analog framework. Section V deals with designing an analog controller for a miniaturized setup by using results from Section III and IV.

¹A microcontroller (or a few microcontrollers) may be used to control an array of miniaturized devices by using Time Multiplexing. In time multiplexing a microcontroller controls each element of the array in a cyclic fashion. In such a scenario a microcontroller will face a huge computational load dependent on the size of the array. Upcoming ideas like "event-based control" promises to reduce the computational load by allowing aperiodic sampling. The motive of this work is not to challenge an existing idea but to propose an alternative one.

²CMOS based hybrid circuits like that proposed in [21] can also act like variable gain control element. However memristors are much smaller (found below 10 nm) than such hybrid circuits and hence ensures better scalability. Gain-Span of memristor is also more than CMOS based hybrid circuits.

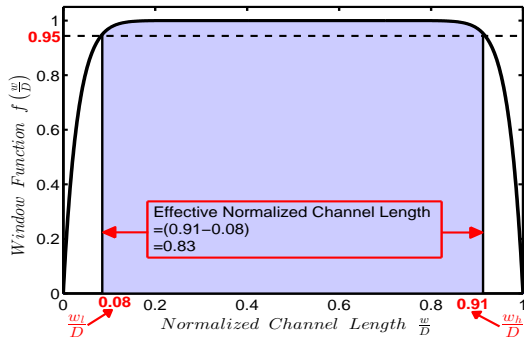


Figure 2. Plot of joglekar window function with $p = 8$ for HP memristor. For a tolerance of 5% in $f(\frac{w}{D})$ the safe zone of operation is $\frac{w}{D} \in [0.08, 0.91]$.

II. MEMRISTOR PRELIMINARIES

Chua [1] postulated the existence of memristor as a missing link in the formulation of electromagnetism. Fig. 1a) gives an intuitive explanation of the same. As evident from Fig. 1a), such an element will link charge Q and flux Φ , i.e. $\Phi = f(Q)$. Differentiating this relation using chain rule and applying Lenz's Law yields

$$V = M(Q)I \quad (1)$$

suggesting that the element will act like a charge controlled variable resistor with $M(Q) = \frac{df}{dQ}$ as the variable resistance. This device has non-volatile memory ([1], [4]) and are hence called memristors. Memristive systems [22] are generalization of memristor with state space representation,

$$\dot{W} = F(W, I); V = R(W, I)I \quad (2)$$

where, W are the internal state variables, I is the input current, V is the output voltage, $R(W, I)$ is the memristance. Memristor reported by HP Labs in [2] is essentially a memristive system with the following state space representation,

$$\dot{w} = \mu \frac{R_{on}}{D} f\left(\frac{w}{D}\right) I; V = \left[R_{on} \frac{w}{D} + R_{off} \left(1 - \frac{w}{D}\right)\right] I \quad (3)$$

It consists of two layers: a undoped region of oxygen-rich TiO_2 and doped region of oxygen-deficient TiO_{2-x} . Doped region has channel length w and low resistance while undoped region has channel length $D - w$ and high resistance. These regions form a series resistance as shown in Fig. 1b. R_{on} and R_{off} are the effective resistance when $w = D$ and $w = 0$ respectively with $R_{off} \gg R_{on}$. μ is the ion mobility. When external bias is applied, the boundary between the two regions drift. This drift is slower near the boundaries, i.e. $\dot{w} \rightarrow 0$ as $w \rightarrow 0$ or $w \rightarrow D$. This nature is captured in [4], [5] using window function $f(\frac{w}{D})$. A plot of Joglekar window function $f(\frac{w}{D}) = 1 - (\frac{2w}{D} - 1)^p$ is shown in Fig. 2. A close investigation of various proposed models [2], [4], [5], [6] reveals two important facts: 1) As shown in Fig. 2, $f(\frac{w}{D})$ is approximately 1, except near the boundaries. 2) Boundary dynamics of memristor is highly non-linear and still a matter of debate. Hence the region $w \in [w_l, w_h]$, $0 < w_l < w_h < D$, where $f(\frac{w}{D}) \approx 1$ is the *safe zone* in which memristor dynamics can be approximated as

$$\dot{Q}_M = I; V = [R_{off}^S - \alpha^S Q_M] I \quad (4)$$

where, $\alpha^S = \frac{(R_{off}^S - R_{on}^S)}{Q_M^S}$, $R_{off}^S = R_{off} - (R_{off} - R_{on}) \frac{w_l}{D}$, $R_{on}^S = R_{on} - (R_{off} - R_{on}) \frac{w_h}{D}$, $D^S = w_h - w_l$, $Q_M^S = \frac{D^S D}{\mu R_{on}}$. Superscript "S" means "safe". In equation (4) we define Q_M such that $Q_M = 0$ when $w = w_l$. Then $Q_M = Q_M^S$ when $w = w_h$. Hence equation (4) is valid when $Q_M \in [0, Q_M^S]$. From now on, the following conventions will be used:

- 1) Memristor would mean a HP memristor operating in safe zone. Memristor dynamics is governed by equation (4).
- 2) The schematic symbol of the memristor shown in Fig. 1a will be used. Conventionally, resistance of memristor decreases as the current enters from the port marked "+".
- 3) HP memristor parameters: $R_{on} = 100\Omega$, $R_{off} = 16k\Omega$, $D = 10nm$, $\mu = 10^{-14} \frac{m^2}{sV}$. We model the memristor using Joglekar Window Function with $p = 8$. The safe zone is marked by $w_l = 0.08D$ and $w_h = 0.91D$ (see Fig. 2) in which $f(\frac{w}{D}) \geq 0.95$. This gives: $R_{off}^S = 15k\Omega$, $R_{on}^S = 1.5k\Omega$, $Q_M^S = 83\mu C$, $\alpha^S = 1.6 \times 10^8 \frac{\Omega}{C}$. These parameters will be used for design purposes.

III. ANALOG GAIN CONTROL FRAMEWORK

In this section we design a AGC circuit whose input-output relation is governed by the following equation,

$$\dot{K} = \alpha_k V_C(t); V_u(t) = K V_e(t) \quad (5)$$

We assume that $K > 0$. This is basically a variable gain proportional controller with output voltage V_u , error voltage V_e and variable gain K . K is controlled by control voltage V_C . α_k determines the sensitivity of V_C on K . An analog circuit following equation (5) is *generic* in the sense that it can be used to implement any gain scheduled control algorithm. We assume V_C and V_e are band limited, i.e. - the maximum frequency component of V_C and V_e are ω_C^M and ω_e^M respectively. Knowledge of ω_C^M and ω_e^M is assumed.

The proposed circuit is shown in Fig. 3. We assume the availability of positive and negative power supply³ V_{DD} and $-V_{DD}$. All op-amps are powered by V_{DD} and $-V_{DD}$.

Claim 1: The proposed circuit shown in Fig. 3. is an *approximate* analog realization of equation (5) if:

- 1) Electrical components in Fig. 3. are ideal. Also for MOSFET's, threshold voltage $V_{th} \approx 0$.
- 2) $\omega_m = 1000 \max\{(\omega_C^M + \omega_e^M), 2\omega_C^M\}$
- 3) $R_f C_f = \frac{100}{\omega_m}$; $R_e C_e = \frac{1}{2(\omega_C^M + \omega_e^M)}$

We understand the working of the proposed circuit by studying its four distinct blocks and in the process prove the above claim. The output response of each block for a given input, V_e and V_C , is shown in Fig. 4. It should be noted that the tuning rules proposed in the claim is only one such set of values which will make the circuit follow equation (5).

Remark 1: Substrate of all NMOS and PMOS are connected to $-V_{DD}$ and V_{DD} respectively. In *ON* state⁴, voltages between $-V_{DD}$ to $(V_{DD} - V_{th})$ will pass through⁵ NMOS and

³ V_{DD} and $-V_{DD}$ are the highest and the lowest potential available in the circuit. From control standpoint, it imposes bounds on control input V_u .

⁴With a slight abuse of terminology, a NMOS and a PMOS is said to be in *ON* state when its gate voltage is V_{DD} and $-V_{DD}$ respectively.

⁵A voltage is said to pass through a MOSFET if the exact voltage applied at its source(drain) terminal appears at its drain(source) terminal.

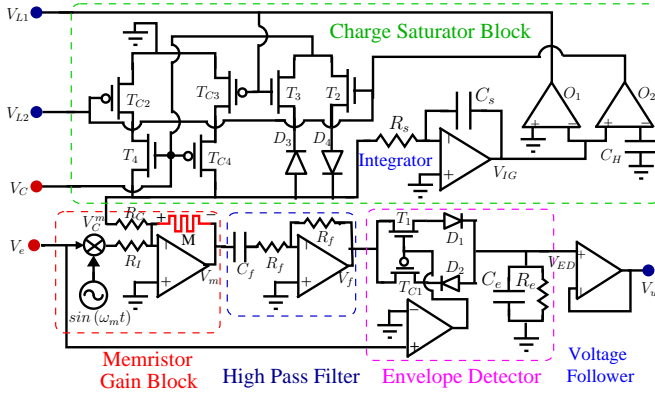


Figure 3. Memristive AGC Circuit. V_e and V_C are the inputs. V_u , V_{L1} and V_{L2} are the outputs. V_{L1} and V_{L2} are zone indicating voltages.

voltages between $-(V_{DD} - V_{th})$ to V_{DD} will pass through PMOS. If $V_{th} \approx 0$, any voltage between $-V_{DD}$ to V_{DD} will pass through NMOS and PMOS when they are in *ON* state.

A. Memristor Gain Block

The key idea of this block has been adapted from [23]. V_C^m and V_e are inputs to this block while V_m is the output. For now we assume $V_C^m = V_C$ (details discussed in III-D). Current I_m through memristor is

$$I_m(t) = \underbrace{\frac{V_e(t) \sin(\omega_m t)}{R_I}}_{I_{noise}} + \underbrace{\frac{V_C(t)}{R_C}}_{I_{ctrl}}$$

From equation (4), resistance of the memristor is given by $M(Q_M) = R_{off}^S - \alpha^S Q_M$. Differentiating this relation we get, $\dot{M} = -\alpha^S I_m(t)$. Hence voltage V_m is given by

$$\dot{M} = -\alpha^S I_m(t); V_m(t) = -I_m(t) M \quad (6)$$

Note that $\omega_m = 1000 \max\{(\omega_C^M + \omega_e^M), 2\omega_C^M\} > \omega_e^M$. In such a case the minimum component frequency of $I_{noise} = \frac{V_e(t) \sin(\omega_m t)}{R_I}$ is $\omega_m - \omega_e^M$. Now

$$\begin{aligned} \omega_m - \omega_e^M &= 1000 \max\{(\omega_C^M + \omega_e^M), 2\omega_C^M\} - \omega_e^M \\ &\geq 1000(\omega_C^M + \omega_e^M) - \omega_e^M \\ &= 1000\omega_C^M + 999\omega_e^M \gg \omega_C^M \end{aligned}$$

This implies that the lowest component frequency of I_{noise} is much greater than the highest component frequency of I_{ctrl} . Also note that $\dot{M} = -\alpha^S I_m(t)$ in an integrator with input $I_m(t)$ and output $M(t)$. As integrator is a low pass filter, the effect of high frequency component I_{noise} on M is negligible compared to I_{ctrl} . Hence equation (6) can be modified as

$$\dot{M} \approx -\frac{\alpha^S}{R_C} V_C(t); V_m(t) = V_m^1 + V_m^2 \quad \text{where,} \quad (7)$$

$V_m^1 = -\frac{M V_e(t)}{R_I} \sin(\omega_m t)$ and $V_m^2 = -\frac{M V_C(t)}{R_C}$. Note V_m^1 is the modulated form of the desired output with gain $K = \frac{M}{R_I}$.

Remark 2: $M(t)$ is the variable gain. According to equation (5), V_e should not effect $M(t)$. Without modulating V_e , the effect of $V_e(t)$ on $M(t)$ would not have been negligible.

B. High Pass Filter (HPF)

The role of HPF is to offer negligible attenuation to V_m^1 and high attenuation to V_m^2 thereby ensuring that the Envelope Detector can recover the desired output.

Note that $M(t)$ is basically the integral of $V_C(t)$. Since integration is a linear operation it does not do frequency translation. Hence the component frequencies of $M(t)$ and $V_C(t)$ are same. Let ω_1^m and ω_2^M denote the minimum component frequency of V_m^1 and maximum component frequency of V_m^2 respectively. Now

$$\begin{aligned} \omega_1^m &= \omega_m - \text{Maximum Frequency Component of } M V_e \\ &= \omega_m - \text{Maximum Frequency Component of } V_C V_e \\ &= \omega_m - (\omega_C^M + \omega_e^M) \end{aligned} \quad (8)$$

$$\begin{aligned} \omega_2^M &= \text{Maximum Frequency Component of } M V_C \\ &= \text{Maximum Frequency Component of } (V_C)^2 \\ &= 2\omega_C^M \end{aligned} \quad (9)$$

The attenuation offered by the HPF is given by $-10 \log(1 + (\omega R_f C_f)^{-2})$ dB. We want to study the attenuation characteristics at two frequencies:

1) At $\omega = \omega_1^m$: At this frequency

$$\begin{aligned} \omega_1^m R_f C_f &= \frac{100(\omega_m - (\omega_C^M + \omega_e^M))}{\omega_m} = 100 \left(1 - \frac{\omega_C^M + \omega_e^M}{\omega_m}\right) \\ &\geq 100 \left(1 - \frac{1}{1000}\right) \approx 100 \end{aligned} \quad (10)$$

Inequality (10) is possible because $\omega_m = 1000 \max\{(\omega_C^M + \omega_e^M), 2\omega_C^M\}$ implying $\frac{\omega_m}{\omega_C^M + \omega_e^M} \geq 1000$. For $\omega_1^m R_f C_f \geq 100$ attenuation is approximately 0dB. As the HPF offers almost no attenuation to the minimum component frequency of V_m^1 , it will offer no attenuation to the higher component frequency of V_m^1 as well. Hence V_m^1 suffers negligible attenuation.

2) At $\omega = \omega_2^M$: At this frequency

$$\omega_2^M R_f C_f = 100 \frac{2\omega_C^M}{\omega_m} \leq \frac{100}{1000} = 0.1 \quad (11)$$

Inequality (11) is possible because $\omega_m = 1000 \max\{(\omega_C^M + \omega_e^M), 2\omega_C^M\}$ implying $\frac{\omega_m}{2\omega_C^M} \geq 1000$. For $\omega_2^M R_f C_f \leq 0.1$ attenuation is more than -20dB. As the HPF offers high attenuation to the maximum component frequency of V_m^2 , it will offer higher attenuation to the lower component frequency of V_m^2 . Hence V_m^2 gets highly attenuated.

As V_m^1 undergoes almost no attenuation (≈ 0 dB), the output of HPF is $V_f = -V_m^1$. The minus sign before V_m^1 is justified as the HPF is in inverting mode.

C. Envelope Detector

The input to this block is $V_f = \frac{M V_e(t)}{R_I} \sin(\omega_m t)$. Similar to amplitude modulation (AM), here $\sin(\omega_m t)$ is the carrier and $\frac{M V_e(t)}{R_I}$ is the signal to be recovered. We use a polarity sensitive envelope detector as $\frac{M V_e(t)}{R_I}$ can be both positive or negative. The key idea used here is that the polarity of V_e and

V_u is same since $K = \frac{M}{R_I} > 0$. Hence we detect the positive peaks of V_f when V_e is positive by keeping T_1 *ON* and T_{C1} *OFF*. When V_e is negative, negative peaks of V_f are detected by keeping T_{C1} *ON* and T_1 *OFF*. Remaining working of the envelope detector is similar to a conventional Diode-based Envelope Detector and can be found in [24]. Effective envelope detection using diode based envelope detector requires:

- 1) $\omega_m \gg \omega_C^M + \omega_e^M$, i.e. the frequency of the carrier should be much greater than the maximum component frequency of the signal. Here $\sin(\omega_m t)$ is the carrier whose frequency is ω_m while $\frac{MV_e}{R_I}$ is the signal whose maximum component frequency is $\omega_C^M + \omega_e^M$ (refer equation (8)).
- 2) $\frac{1}{\omega_m} \ll R_e C_e$, i.e. the time constant of the envelope detector is much larger than the time period of the modulating signal. This ensures that the capacitor C_e (refer Fig. 3) discharges slowly between peaks thereby reducing the ripples.
- 3) $R_e C_e < \frac{1}{\omega_C^M + \omega_e^M}$, i.e. the time constant of the envelope detector should be less than the time period corresponding to the maximum component frequency of the signal getting modulated. This is necessary so that the output of the envelope detector can effectively track the envelope of the modulated signal.

The proposed tuning rule in *Claim 1* satisfies these conditions. In general, for amplitude modulation (AM) the choice of modulating frequency is 100 times the maximum component frequency of the signal getting modulated. Unlike AM, our multiplying factor is 1000 instead of 100. The reason for choosing this should be clearly understood. In a conventional diode based peak detector the ripple in output voltage can be decreased either by increasing the modulating frequency ω_m or by increasing the time constant $R_e C_e$. But $R_e C_e$ is upper bounded by $\frac{1}{\omega_C^M + \omega_e^M}$. In our case the signal to be modulated, i.e. $\frac{MV_e}{R_I}$, may contain frequencies anywhere in the range $[0, \omega_C^M + \omega_e^M]$. For a given $R_e C_e$ a signal with a lower frequency will suffer higher ripple. Hence to constrain the ripple for any frequency in the specified range one must constrain the ripple for 0 frequency (DC voltage). For DC voltage ripple factor is approximately $\frac{2\pi \times 100}{\sqrt{3} \omega_m R_e C_e}$. With the choice of $R_e C_e$ made in Claim 1 and 100 as multiplying factor, ripple factor is as large as 7.2%. Therefore, we choose multiplying factor of 1000 which gives a ripple factor of 0.72%. The output of the envelope detector is $\frac{MV_e(t)}{R_I}$ and the final output of the circuit is

$$\dot{M} \approx -\frac{\alpha^S}{R_I R_C} V_C(t); V_u(t) = M V_e \quad (12)$$

where, $M = \frac{M}{R_I}$. Comparing equations (5) and (12) we see that $\alpha_k = -\frac{\alpha^S}{R_I R_C}$ and $K = M$ where $M \in \left[\frac{R_{on}^S}{R_I}, \frac{R_{off}^S}{R_I} \right]$. R_I is tuned to get the desired range of gain while R_C is a free parameter which can be tuned according to the needs.

D. Charge Saturator Block

This block limits the memristor to work in its safe zone hence ensuring validity of equation (4). In safe zone the

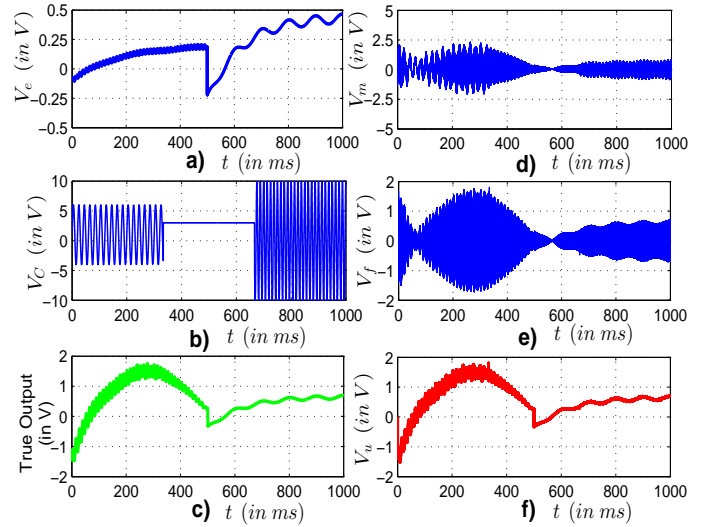


Figure 4. Output of various stages of the circuit shown in Fig. 3, i.e. V_m , V_f and V_u , corresponding to inputs: V_e and V_C . Parameters of simulations are: HP Memristor in safe zone, $\omega_m = 628 \times 10^3 \text{ rads}^{-1}$, $R_C = 100 \text{ k}\Omega$, $R_I = 1 \text{ k}\Omega$, $R_f C_f = 0.159 \text{ ms}$, $R_e C_e = 0.796 \text{ ms}$, $V_{DD} = 5 \text{ V}$, $R_s C_s = 0.826 \text{ s}$. V_u is obtained by simulating the circuit show in Fig. 3. The *true output* is obtained by numerically solving equation (5). In both cases we use V_e and V_C shown in Fig. 4a and Fig. 4b respectively as inputs.

following equations are valid⁶,

$$\frac{dV_{IG}}{dt} = -\frac{V_C^m}{R_s C_s}; \frac{dQ_M}{dt} = \frac{V_C^m}{R_C} \Rightarrow \frac{dV_{IG}}{dQ_M} = -\frac{R_C}{R_s C_s} \quad (13)$$

Recall that in the safe zone $w \in [w_l, w_h]$ and $Q_M \in [0, Q_M^S]$. We assume that integrator voltage $V_{IG} = 0$ when $Q_M = 0$ (or $w = w_l$). Integrating equation (13) under this assumption yields

$$V_{IG} = -\frac{R_C}{R_s C_s} Q_M \quad (14)$$

In equation (14), if $Q_M = Q_M^S$ (or $w = w_h$), $V_{IG} = -\frac{R_C Q_M^S}{R_s C_s}$. Hence, $V_{IG} \in \left[-\frac{R_C Q_M^S}{R_s C_s}, 0 \right]$ when memristor is in its safe zone. In Fig. 3 comparator O_1 and O_2 are used to compare V_{IG} to know if the memristor is in safe zone. Note that: 1) Reference voltage of comparator O_1 and O_2 is GND and voltage V_H (across capacitor C_H) respectively. V_H is set to $-\frac{R_C Q_M^S}{R_s C_s}$ by Synchronization Block (refer Section III-E). 2) In Fig. 3 any MOSFET transistor couple, T_i and T_{C_i} , are in complementary state, i.e. if T_i is *ON*, T_{C_i} will be *OFF* and vice-versa. 3) Comparator output V_{L1} and V_{L2} gives knowledge about the state of the memristor. Also $V_{L1}, V_{L2} \in \{-V_{DD}, V_{DD}\}$. Now depending on V_{L1} and V_{L2} , three different cases may arise:

Case 1 ($V_H < V_{IG} < 0 \Rightarrow V_{L1} = V_{DD}, V_{L2} = V_{DD}$) This implies that the memristor is in its safe zone, i.e. $0 < Q_M < Q_M^S$. Q_M can either increase or decrease. Hence both T_2 and T_3 are *ON* allowing both positive and negative voltage to pass through, i.e. $V_C^m = V_C$.

Case 2 ($V_{IG} < V_H \Rightarrow V_{L1} = V_{DD}, V_{L2} = -V_{DD}$) This happens when $Q_M \geq Q_M^S$. Since Q_M can only decrease, T_2 is kept *OFF* but T_3 is *ON*. Two cases are possible: if

⁶Actually, $\frac{dQ_M}{dt} = \frac{V_C^m}{R_C} + \frac{V_e \sin(\omega_m t)}{R_I}$. But as proved in III-A, the effect of high frequency term, $V_e \sin(\omega_m t)$ on Q_M is negligible.

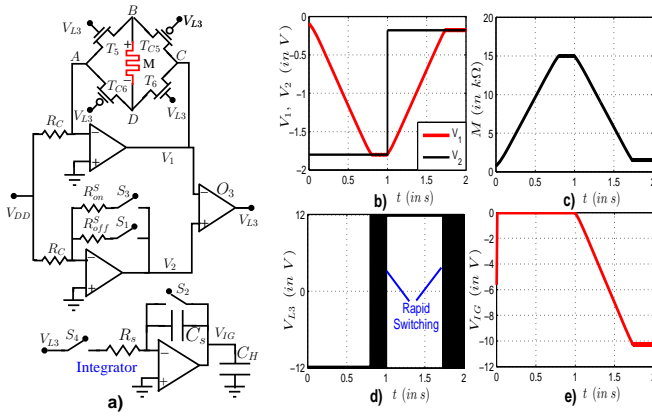


Figure 5. a) Schematic of Synchronization Block. b), c), d), e) Graphs showing operations of Synchronization Block. In these graphs preset mode operates for the first 1s and online calibration mode operates for the next 1s.

$V_C > 0$, T_4 and T_{C2} will be *ON* making $V_C^m = 0$ or $V_C < 0$ making it pass through T_3 and thereby setting $V_C^m = V_C$.

Case 3 ($V_{IG} > 0 \Rightarrow V_{L1} = -V_{DD}$, $V_{L2} = V_{DD}$)

This happens when $Q_M \leq 0$. Since Q_M can only increase, T_3 is kept *OFF* but T_2 is *ON*. Two cases are possible: if $V_C < 0$, T_{C4} and T_{C3} will be *ON* making $V_C^m = 0$ or $V_C > 0$ making it pass through T_2 and thereby setting $V_C^m = V_C$.

E. Synchronization Block

Operation of Charge Saturator Block assumes that: 1) $V_{IG} = 0$ when $Q_M = 0$ (or $w = w_l$). 2) Voltage V_H across capacitor C_H equals $-\frac{R_C Q_M^S}{R_s C_s}$. This block ensures these two conditions and thereby guarantees that the memristor and the integrator in Fig. 3 are in ‘‘synchronization’’. Synchronization Block is shown in Fig. 5a). In Fig. 5a, the op-amp with the memristor, the integrator and capacitor C_H are indeed part of the circuit shown in Fig. 3. Such a change in circuit connection is possible using appropriate switching circuitry. This block operates in two modes:

Preset Mode: We first ensure that $V_{IG} = 0$, when $w = w_l$. In this mode switch S_1 and S_2 are *ON* and switch S_3 and S_4 are *OFF*. When S_2 is closed the residual charge in capacitor C_H will get neutralized thus ensuring $V_{IG} = 0$. Next we make $w = w_l$. Note that $V_1 = -\frac{M V_{DD}}{R_C}$ and $V_2 = -\frac{R_{off}^S V_{DD}}{R_C}$. If $M < R_{off}^S$ then $V_1 > V_2 \Rightarrow V_{L3} = -V_{DD}$. Hence the path *ADBC* of wheatstone bridge arrangement will be active making the current flow from $(-)^{ve}$ to $(+)^{ve}$ terminal of the memristor. This will increase M till $M = R_{off}^S$. If $M > R_{off}^S$, the path *ABDC* is active making M decrease till $M = R_{off}^S$.

Online Calibration⁷: Immediately after preset mode is complete, S_1 and S_2 are switched *OFF* and S_3 and S_4 are switched *ON*. Now, $V_1 = -\frac{M V_{DD}}{R_C}$ and $V_2 = -\frac{R_{on}^S V_{DD}}{R_C}$. In this step $V_{L3} = V_{DD}$ as $M > R_{on}^S$ always. Path *ABDC* will be active driving M to R_{on}^S . As V_{L3} is given as an

⁷If we tune R_s and C_s s.t. $-\frac{R_C Q_M^S}{R_s C_s} = -V_{DD}$, $V_{IG} \in [-V_{DD}, 0]$ when memristor is in safe zone. Then we can directly use power supply $-V_{DD}$ as the reference voltage for comparator O_2 . This will eliminate the need of capacitor C_H and ‘‘Online Calibration’’. However if $-\frac{R_C Q_M^S}{R_s C_s} \neq -V_{DD}$ (due to tuning error), this approach may drive the memristor to non-safe zone.

input to the integrator, capacitor C_H will also get charged. Note that in this step memristor will work in safe zone. Also $V_{IG} = 0$ when $Q_M = 0$ (ensured by preset mode). Hence relation between V_{IG} and Q_M will be governed by equation (14). When M gets equalized to R_{on}^S , $Q_M = Q_M^S$, thereby making $V_H = V_{IG} = -\frac{R_C Q_M^S}{R_s C_s}$.

Each of the modes operate for a predefined time. The resistors and hence the voltages V_1 and V_2 may get equalized before the predefined time after which V_{L3} will switch rapidly. Such rapid switching can be prevented by replacing the comparator O_3 by a cascaded arrangement of a differential amplifier followed by a hysteresis block.

Various graphs corresponding to synchronization process are shown in Fig. 5 b), c), d), e). Memristor Gain Block and the Integrator of Charge Saturator Block should be periodically synchronized to account for circuit non-idealities. One such non-ideality can be caused if the capacitor C_H is leaky causing the voltage V_H to drift with time.

Remark 3: In the discussion of the Synchronization Block we have slightly misused the symbols R_{on}^S and R_{off}^S . Resistance of R_{on}^S and R_{off}^S shown in Fig. 5a should be close to the actual R_{on}^S and R_{off}^S (as mentioned in Section II) respectively. It is not necessary that they should be exactly equal. However, there resistance must lie within the safe zone. This alleviates analog implementation by eliminating the need of *precision resistors*. It should be noted that the maximum and the minimum resistance of the memristor in safe zone is governed by the resistances R_{on}^S and R_{off}^S used in the Synchronization Block *not* the actual R_{on}^S and R_{off}^S .

To conclude, in this section we designed an Analog Gain Control framework using Memristor. Schematic of Memristive AGC is shown in Fig. 2 whose circuit parameters can be tuned using *Claim 1*. Memristive AGC’s designed in this work is ‘‘generic’’ in the sense that it can be used to implement several Gain-Scheduled control algorithms.

IV. CONTROL STRATEGY

As mentioned in the introduction, we are interested in designing Robust Adaptive Control Algorithms to tackle issues like parameter uncertainty (caused by design errors) and time varying nature (caused by ageing effect and atmospheric variation). ‘*Simplicity*’ is the key aspect of any control algorithm to be implementable in analog framework as we do not have the flexibility of ‘*coding*’. Robust Adaptive Control Algorithms found in control literature cannot be implemented in an analog framework due to their complexity. Here we propose a simple gain-scheduled robust adaptive control algorithm which can be easily implemented using Memristive AGC discussed in Section III. We prove the stability of the proposed algorithm using *Lyapunov-Like* method in Section IV-A.

Notations: The notations used in this paper are quite standard. \mathbb{R}^+ and \mathbb{R}^n denotes the set of positive real numbers and the n -dimensional real space respectively. I represents identity matrix of appropriate dimension. $|\cdot|$ is the absolute value operator. \emptyset represents a null set. The bold face symbols \mathcal{S} and \mathcal{S}^+ represents the set of all symmetric matrices and positive definite symmetric matrices respectively. $\inf(\cdot)$ ($\sup(\cdot)$)

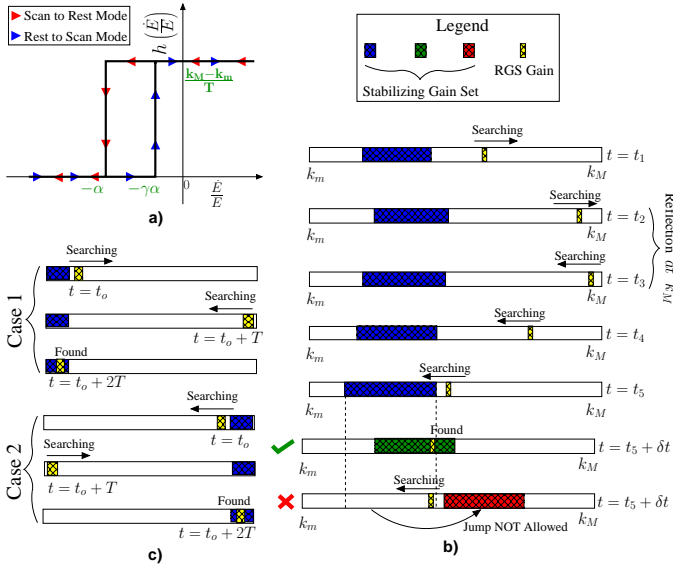


Figure 6. a) Hysteresis Function as mentioned in equation (16). T is the scan time. $\alpha \in \mathbb{R}^+ - \{0\}$ and $\gamma \in [0, 1)$ are tuning constants. b) First six images shows the scan/rest mode of RGS. The last three images depicts the concept of *drifting*. c) Figure showing the worst case scan time.

represents the infimum (supremum) of a set. For a matrix A , $\lambda_m(A)$ and $\lambda_M(A)$ denotes the minimum and maximum eigenvalue of A respectively. $A \preceq B$ implies $B - A$ is positive semi-definite while $A \prec B$ implies $B - A$ is positive definite. The euclidean norm of a vector and the induced spectral norm of a matrix is denoted $\|\cdot\|$. The operator \times when applied on sets implies the cartesian product of the sets. $\text{Conv}\{A\}$ implies the convex hull of set A . Analysis presented further in this paper uses ideas from real analysis, linear algebra and convex analysis. For completeness, these ideas are briefly reviewed in Appendix C.

A. Reflective Gain Space Search (RGS)

Consider a SISO uncertain linear time variant (LTV) system with states $x = [x_1 \ x_2 \ \dots \ x_N]^T \in \mathbb{R}^N$, input $u \in \mathbb{R}$ and output $y \in \mathbb{R}$ described by the following state space equation

$$\dot{x} = A(t)x + B(t)u; \quad y = Cx = x_1 \quad \text{where,} \quad (15)$$

$$A(t) = \begin{bmatrix} 0 & 1 & \dots & 0 \\ \vdots & \vdots & \ddots & \vdots \\ 0 & 0 & \dots & 1 \\ a_1(t) & a_2(t) & \dots & a_N(t) \end{bmatrix} \quad B(t) = \begin{bmatrix} 0 \\ \vdots \\ 0 \\ b(t) \end{bmatrix}$$

The output matrix $C = [1 \ \dots \ 0 \ 0]$.

Assumptions:

- 1) The order N of the system is known.
- 2) The variation of $a_i(t)$, $\forall i = 1, 2, \dots, N$ and $b(t)$ due to parameter uncertainty and time variation is bounded, i.e. $(A(t), B(t))$ belongs to a bounded set \mathcal{L} . \mathcal{L} is assumed to be a connected set. $A(t)$ and $B(t)$ are not known but knowledge of \mathcal{L} is assumed. This assumption basically means that we don't have knowledge about $a_i(t)$ and $b(t)$ however we know the *range* in which they lie.
- 3) $\|\dot{A}\| \leq \delta_A$ and $\|\dot{B}\| \leq \delta_B$. Knowledge of δ_A and δ_B is assumed. This assumption basically means that $A(t)$ and $B(t)$ are continuous in time.

- 4) Let $b(t) \in [b_l, b_u]$ s.t. $b_l \leq b_u$, and either $b_l > 0$ or $b_u < 0$. This choice of b_l and b_u is explained in Section IV-B.

Example to clarify the concept of \mathcal{L} , δA and δB is dealt later in Section IV-B however we give the following example to better explain *Assumption 4*.

Example 1: Consider two cases: 1) $b(t) \in [-2, 3]$ 2) $b(t) \in [0.5, 3]$. According to *Assumption 4*, *Case 2* is possible while *Case 1* is not. This example clearly illustrates that according to *Assumption 4* the sign of $b(t)$ does not change with time and is known with absolute certainty. Note that sign of $b(t)$ decides the sign of static gain⁸ of the system. So *Assumption 4* in certain sense means that the sign of static gain does not change with time and is known with absolute certainty. For all practical scenario such an assumption is valid.

Notice that all assumptions are mild from practical viewpoint. Our aim is to regulate the output around the operating point $y^* = x_1^* = r$. Conventional set-point control consist of a bias term $u_b(t)$ plus the regulation control input $u_r(t)$, i.e. $u(t) = u_b(t) + u_r(t)$. Here we assume that $u_b(t)$ is designed s.t. $x^* = [r \ 0 \ \dots \ 0]^T$ is the equilibrium point and concentrate on the synthesis of $u_r(t)$. For simplicity we consider $r = 0$, i.e. $x^* = [0 \ 0 \ \dots \ 0]^T$ is the equilibrium point. As we are dealing with a linear system the same analysis is valid for $r \neq 0$. The controller structure is, $u_r(t) = -K(t)y(t)$, where $K(t) \in [k_m, k_M]$ is the variable gain s.t. $0 < k_m < k_M$. Let $E = x^T P x$ be the Lyapunov Candidate Function⁹ with $P \in \mathbf{S}^+$. Then RGS is as simple Gain-Scheduled control strategy given by the following equation

$$\dot{K} = \text{sgn} \cdot h\left(\frac{\dot{E}}{E}\right); \quad u_r = -Ky \quad (16)$$

where, $\text{sgn} \in \{-1, 1\}$ and $h\left(\frac{\dot{E}}{E}\right)$ is a hysteresis function shown in Fig. 6a. Working of RGS can be explained as:

- 1) RGS finds the stabilizing gain¹⁰, i.e. the gain which renders $\dot{E} < 0$ ($\dot{E} < -\alpha E$ in a more strict sense), by reflecting back and forth between $[k_m, k_M]$. RGS is said to be in "Scan Mode" when it is scanning for the stabilizing gain. It goes to "Rest Mode" when stabilizing gain is found. RGS Scan Cycle is clearly depicted in the first six images of Fig. 5b).
- 2) RGS uses \dot{E} as stability indicator. \dot{E} is found by differentiating E which in turn is calculated using $E = x(t)^T P x(t)$. To get the states $x(t)$ we differentiate the output $y(t)$ $N - 1$ times.
- 3) Scan Mode is triggered when $\dot{E} > -\gamma\alpha E$ (refer Fig. 6a). Scan Mode is associated with a scan time of T , i.e. time taken to scan from k_m to k_M . Hence, $h\left(\frac{\dot{E}}{E}\right) = \frac{k_M - k_m}{T}$. The value of sgn is 1 when gain space is searched from k_m to k_M and -1 otherwise. Scan mode operates till $\dot{E} > -\alpha E$.

⁸Unlike LTI system, static gain for LTV system may not be well defined. Here we define static gain of LTV system (15) as $\frac{b(t)}{a_1(t)}$.

⁹Use of time invariant Lyapunov Function to analyse stability of LTV systems has been used in [25] (Chap. 5, 7) and [26] (Chap. 3).

¹⁰The term "stabilizing gain" has been slightly misused. Stability of LTV system cannot be assured even if the closed loop system matrix, $A(t) - B(t)K(t)C$, has negative real eigen part for all $t > 0$ ([27], [28]).

- 4) Rest Mode is triggered when $\dot{E} < -\alpha E$. In this mode $h\left(\frac{\dot{E}}{E}\right) = 0$, i.e. the stabilizing gain is held constant. Rest mode operates till $\dot{E} < -\gamma\alpha E$.
- 5) In the process of finding stabilizing gain, LTV system may expand (E increases) in Scan Mode and will contract (E decreases) in Rest Mode. RGS ensures that even in the worst case, contraction is always dominant over expansion, guaranteeing stability.

Stabilizing Gain Set¹¹ $\mathcal{K}_{P,s}(t)$ for a given $P \succ 0$ and $s \in \mathbb{R}^+$ at time t is defined as

$$\mathcal{K}_{P,s}(t) = \left\{ K \in \mathbb{R} : A_C(t)^T P + P A_C(t) \preceq -sI, \right. \\ \left. A_C(t) = A(t) - B(t)KC, k_m \leq K \leq k_M \right\}$$

Lemma 1: If $\mathcal{K}_{P,s}(t) \neq \emptyset, \forall t \geq 0$ then under *Assumption 3*, $\mathcal{K}_{P,s}(t) \cap \mathcal{K}_{P,s}(t + \delta t) \neq \emptyset$ if $\delta t \rightarrow 0$.

Proof: This lemma basically means that stabilizing gain set will drift. If the stabilizing gain set is drifting then there will be an intersection between stabilizing gain sets at time t_1 and t_2 if $t_2 - t_1$ is small. Drifting is obvious under *Assumption 3* however a formal proof is given in Appendix A.

Concept of ‘‘drifting’’ is clearly depicted in the last three images of Fig. 5b. Notice that at $t = t_5$ the stabilizing gain set is almost found. Two possible cases are shown in Fig. 5b for $t = t_5 + \delta t$ where $\delta t \rightarrow 0$. In the first case the stabilizing gain set is drifting while in the other case the stabilizing gain set jumps. In the first case the stabilizing gain is found and RGS goes to Rest Mode. In the second case RGS will just miss the stabilizing gain set. Hence if the stabilizing set keeps jumping, the scan mode may never end. Hence if the stabilizing set keeps jumping, the scan mode may never end. As mentioned in *Lemma 1*, stabilizing set $\mathcal{K}_{P,s}(t)$ never jumps if *Assumption 3* is valid. Therefore *Lemma 1* is important to guarantee an upper bound on the time period of Scan Mode from which we get the following Lemma.

Lemma 2: If $\mathcal{K}_{P,s}(t) \neq \emptyset, \forall t \geq 0$ then under *Assumption 3*, the maximum time period of Scan Mode is $2T$.

Proof: It is a direct consequence of *Lemma 1*. The worst case time period of $2T$ happens only in two cases. Both the cases are shown in Fig. 6c.

Theorem 1: LTV system characterized by equation (15) and set \mathcal{L} is stable under RGS Control Law proposed in equation (16) if it satisfies the following criterion

- 1) **[C1]** If corresponding to all $(A, B) \in \mathcal{L}$ there exist atleast one gain $K_{AB} \in [k_m, k_M]$ s.t.

$$(A - BK_{AB}C)^T P + P(A - BK_{AB}C) \preceq -sI \quad (17)$$

for some $s \in \mathbb{R}^+$.

- 2) **[C2]** Scan time $T < \frac{\lambda_m(P)\alpha^2(1-\gamma^2)}{8\delta \max(\lambda_M^c, 0)}$. Here $\gamma \in [0, 1)$, $\delta = \delta_A + \delta_B k_M$ and $\lambda_M^c = \max_{Q \in S_Q^c} \lambda_M(Q)$ where the set

$$S_Q^c = \left\{ Q : Q = (A - BKC)^T P + P(A - BKC) \right. \\ \left. (A, B) \in \mathcal{L}, K \in [k_m, k_M] \right\}$$

¹¹The stabilizing gain set $\mathcal{K}_{P,s}(t_o)$ at time $t = t_o$, is just a ‘‘Lyapunov-Way’’ of describing the set of gains which will stabilize the corresponding LTI system $(A(t_o), B(t_o), C)$ at time $t = t_o$.

Proof: Consider the Lyapunov candidate $E = x^T P x$ which when differentiated along systems trajectory yields

$$\dot{E} = x^T Q(t) x \leq \lambda_M(Q(t)) \|x\|^2 \leq \lambda_M^c \|x\|^2 \quad (18)$$

where, $Q(t) = A_C(t)^T P + P A_C(t)$ and $A_C(t) = A(t) - B(t)K(t)C$. Definitely, $Q(t) \in \mathbf{S}$ as it is a sum of the matrix $P A_C(t)$ and its transpose $A_C(t)^T P$. Note that, $\lambda_M(Q(t)) \leq \lambda_M^c, \forall (A, B) \in \mathcal{L}$ and $\forall K \in [k_m, k_M]$. When $\lambda_M^c < 0$, stability is obvious as according to inequality (18) $\dot{E} < 0, \forall (A, B) \in \mathcal{L}$ and $\forall K \in [k_m, k_M]$. As $\dot{E} < 0$ for any $\forall K \in [k_m, k_M]$, stability is guaranteed even if scanning is infinitely slow, i.e. scan time $T \rightarrow \infty$. This is in accordance with **[C2]**.

We now consider the case when $\lambda_M^c > 0$. Say at time $t = t^*$, $E = E^*$ and the system goes to scan mode to search for a stabilizing gain. From inequality (18) we have,

$$\dot{E} \leq \lambda_M^c \|x\|^2 \leq \frac{\lambda_M^c}{\lambda_m(P)} E \quad (19)$$

We want to find the maximum possible increase in E in the Scan Mode. At this point it is important to understand that **[C1]** is another way of saying that $\mathcal{K}_{P,s}(t) \neq \emptyset, \forall t \geq 0$. Hence if **[C1]** is true, then *Lemma 2* can be used to guarantee that the maximum period of scan mode is $2T$. Let $E = E_s$ and $t = t_s$ at the end of scan mode. Maximum expansion in E is obtained by integrating inequality (19) from $t = t^*$ to $t = t^* + 2T$

$$E_S \leq \beta_s E^* \quad \text{where,} \quad (20)$$

$\beta_s = \exp\left(\frac{2\lambda_M^c T}{\lambda_m(P)}\right)$, the worst case expansion factor. The end of scan mode implies that a stabilizing gain is found, i.e. at $t = t_s, \dot{E}(t_s) \leq -\alpha E(t_s)$ (refer Fig. 6a), and the rest mode starts. Here it is important to note the relation between α and s (refer **[C1]**). **[C1]** assures that at $t = t_s$ a gain K can be found s.t.

$$\dot{E}(t_s) \leq \lambda_M(Q(t_s)) \|x\|^2 = -s \|x\|^2 \\ \leq -\frac{s}{\lambda_M(P)} E(t_s) \quad (21)$$

Comparing inequality (21) with Fig. 6a we get $\alpha = \frac{s}{\lambda_M(P)}$.

Let τ be the duration of rest mode. We want to find the minimum possible decrease in E in rest mode before it again goes back to scan mode. Again,

$$\dot{E} = x^T Q(t) x = x^T [Q(t_s) + \Delta(t)] x \\ = \dot{E}(t_s) + x^T \Delta(t) x \quad \text{where,} \quad (22)$$

$\Delta(t) = Q(t) - Q(t_s)$. As $K(t) = K(t_s); t_s \leq t \leq t_s + \tau$ ($\dot{K} = 0$ in rest mode), $\Delta(t)$ can be expanded as

$$\Delta(t) = [\Delta A(t) - \Delta B(t)K(t_s)C]^T P \\ + P[\Delta A(t) - \Delta B(t)K(t_s)C] \quad (23)$$

where, $\Delta A(t) = A(t) - A(t_s)$ and $\Delta B(t) = B(t) - B(t_s)$. Taking norm on both side of equation (23) yields

$$\|\Delta(t)\| \leq 2 \|P[\Delta A(t) - \Delta B(t)K(t_s)C]\| \\ \leq 2 \|P\| (\|\Delta A(t)\| + \|\Delta B(t)\| \|K(t_s)\| \|C\|) \\ \leq 2\lambda_M(P) \delta \Delta t \quad (24)$$

where, $\delta = \delta_A + \delta_B k_M$ and $\Delta t = t - t_s$. Note that $\|C\| = 1$. Also $\|P\| = \lambda_M(P)$ for all $P \in \mathbf{S}^+$. Getting back to equation (22) we have

$$\begin{aligned} \dot{E} &= \dot{E}(t_s) + x^T \Delta(t) x \leq -s \|x\|^2 + \|\Delta(t)\| \|x\|^2 \\ &\leq -s \|x\|^2 + \|\Delta(t)\| \|x\|^2 \\ &\leq -[s - 2\lambda_M(P) \delta \Delta t] \|x\|^2 \\ &\leq -(\alpha - 2\delta \Delta t) E \end{aligned} \quad (25)$$

To find the minimum possible value of τ we can substitute $\dot{E} = -\gamma \alpha E$ in inequality (25). This gives,

$$\tau \geq \frac{\alpha(1-\gamma)}{2\delta} \quad (26)$$

Hence, $\tau_{min} = \frac{\alpha(1-\gamma)}{2\delta}$. Let $E = E_r$ at the end of rest mode. We integrate inequality (25) from $t = t_s$ to $t = t_s + \frac{\alpha(1-\gamma)}{2\delta}$ to find the minimum possible contraction in rest mode,

$$E_r \leq \beta_r E_s \quad \text{where,} \quad (27)$$

$\beta_r = \exp\left(-\frac{\alpha^2(1-\gamma^2)}{4\delta}\right)$, the worst case contraction factor. Using inequality (20) and (27) we get

$$E_r \leq \beta E^* \quad \text{where,} \quad (28)$$

$\beta = \beta_s \beta_r = \exp\left(-\frac{\alpha^2(1-\gamma^2)}{4\delta} + \frac{2\lambda_M^c T}{\lambda_m(P)}\right)$. If $\beta \in (0, 1)$, there will be an overall decrease in E in a rest-scan cycle. $\beta \in (0, 1)$ can be assured if

$$T < \frac{\lambda_m(P) \alpha^2 (1-\gamma^2)}{8\delta \lambda_M^c} \quad (29)$$

Now we want to prove that inequality (29) ensures that $E(t) \rightarrow 0$ (and hence¹² $x(t) \rightarrow 0$) as $t \rightarrow \infty$. Before proceeding forward we note two things: 1) Theoretically predictable duration of a rest-scan cycle is $T_{rs} = 2T + \frac{\alpha(1-\gamma)}{2\delta}$. 2) T_{rs} is a conservative estimate of the duration of a rest-scan cycle. Hence it may as well happen that the rest mode lasts for a longer time leading to unpredictable contraction. This is clearly shown in Fig. 7. Now we want to put an upper bound on $E(t)$. Say we want to upper bound $E(t)$ in any one blue dots shown in Fig. 7, i.e. in the green zones. This can be done as follows

$$E(t) \leq E_o \beta^{\eta(t)} \exp(-\gamma \alpha (t - \eta(t) T_{rs})) \quad (30)$$

where, $E = E_o$ at $t = 0$, $\eta(t)$ is the number of complete rest-scan cycle¹³ before time t . In inequality (30), $\beta^{\eta(t)}$ is the predictable contraction factor contributed by the red zones in Fig. 7 and the last term is the unpredictable contraction factor contributed by the green zones in Fig. 7. Note that in green zones all we can assure is that, $\dot{E} \leq -\gamma \alpha E$, which when integrated yields the last term of inequality (30). Now we want to upper bound $E(t)$ in one of the red dots shown in Fig. 7 which can be done as

¹²As $E = x^T P x \geq \lambda_m(P) \|x\|^2$ it implies $\|x\| \leq \sqrt{\frac{E}{\lambda_m(P)}}$ where $\lambda_m(P) > 0$ as $P \succ 0$. Hence if $E \rightarrow 0$ then $\|x\| \rightarrow 0$ implying $x \rightarrow 0$.

¹³Without additional knowledge of system dynamics, $\eta(t)$ is not predictable.

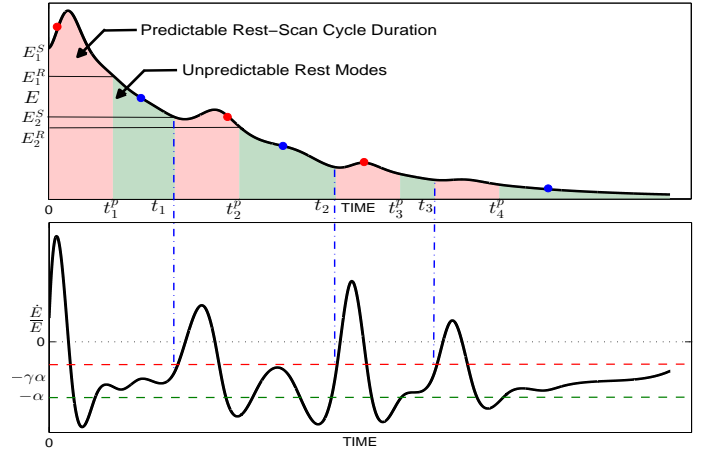


Figure 7. Plot showing the actual and predictable duration of rest-scan cycle. Red zones shows the predictable duration, i.e. $(t_i^p - t_{i-1}^p) = T_{rs}$, while the actual duration is $t_i - t_{i-1}$. Also note that $E_i^R \leq \beta E_i^S$, the theoretically predictable contraction in a rest-scan cycle. The green zones shows the unpredictable rest modes.

$$E(t) \leq E_o \beta_s \beta^{\eta(t)} \exp\left(-\gamma \alpha (t - T_{rs} - \eta(t) T_{rs})^+\right) \quad (31)$$

In inequality (31), the operator $(a)^+ = \max(0, a)$. Inequality (31) resembles (30) except that in this case the system may be in scan mode leading to the extra expansion factor β_s in the expression. There is an extra $-T_{rs}$ in the last term to deduct the predictable time of the current rest-scan cycle. Among inequality (30) and (31), (31) is definitely the worst case upper bound on $E(t)$ due to the presence of two additional terms, i.e. $-T_{rs}$ inside $\exp(-\gamma \alpha (\cdot))$ and $\beta_s \geq 1$. From inequality (31) it is clear that if $\beta \in (0, 1)$ then, $E(t) \rightarrow 0$ as $t \rightarrow \infty$. This completes the proof of Theorem 1.

Remark 4: From inequality (31) convergence is better if β is small. According to inequality (28), β decreases as α (or s) increases and T decreases. The effect of γ on β is more involved. In inequality (31), if γ increases then β increases (refer inequality (28)). Thus predictable contraction decreases (due to large β) but unpredictable contraction increases (due to large γ). Hence γ can be neither too high nor too low.

Remark 5: Note that RGS strategy doesn't impose any theoretical limit on the rate of variation, δ_A and δ_B , of LTV system. This is perhaps one of the novelty of RGS.

Remark 6 (RGS for LTI Systems): For uncertain LTI systems, Theorem 1 will have [C1] without any change. However, [C2] will no longer impose an upper bound on T but will just demand a finite non-zero value. This will ensure that a stabilizing gain is found within a finite time period of $2T$.

B. Bilinear Matrix Inequality(BMI) Optimization Problem

Foundation of RGS is based on the validity of [C1] for a given uncertain LTV/LTI system. We pose a BMI optimization problem to check the validity of [C1] and in the process find the value of P and s needed for implementing RGS.

We start our discussion by formally defining the set \mathcal{L} . Let $A(t)$ and $B(t)$ be functions of p independent physical parameters $\Theta = [\Theta_1, \Theta_2, \dots, \Theta_p]^T$, i.e. $(A(t), B(t)) = F(\Theta(t))$. $\Theta(t)$ is time varying and at every time instant is

also associated with a uncertainty set because of parameter uncertainty. We assume that every physical parameter Θ_i is bounded, i.e. $\Theta_i(t) \in [\Theta_i^L, \Theta_i^H]$. Then $\Theta(t) \in \mathcal{S}$, where $\mathcal{S} = [\Theta_1^L, \Theta_1^H] \times [\Theta_2^L, \Theta_2^H] \times \dots \times [\Theta_p^L, \Theta_p^H]$ a p -dimensional hypercube. We assume no knowledge of the time variation of Θ , i.e. $\Theta(t)$, but we assume the knowledge of \mathcal{S} . Then \mathcal{L} is the image of \mathcal{S} under the transformation F , i.e. $F: \mathcal{S} \rightarrow \mathcal{L}$ where $\mathcal{S} \subset \mathbb{R}^p$ and $\mathcal{L} \subset \mathbb{R}^{N \times N} \times \mathbb{R}^{N \times 1}$.

Remark 7: The system described by equation (15) can be represented using the compact notation $[a_1 \ a_2 \ \dots \ a_N \ | \ b]$. Hence one can assume that $\mathcal{L} \subset \mathbb{R}^{N+1}$ rather than $\mathcal{L} \subset \mathbb{R}^{N \times N} \times \mathbb{R}^{N \times 1}$. This reduces notational complexity by making the elements of \mathcal{L} a vector rather than ordered pair of two matrix.

At this point we would be interested in formulating **[C1]** as an optimization problem. With a slight misuse of variable s we can state the following problem.

Problem 1: **[C1]** holds if and only if the optimal value of the problem

minimize: s

subject to:

$$(A - BK_{AB}C)^T P + P(A - BK_{AB}C) \preceq sI \quad \forall (A, B) \in \mathcal{L}$$

$$P \succ 0$$

with the design variables $s \in \mathbb{R}$, $P \in \mathbb{R}^{N \times N}$ and $K_{AB} \in [k_m, k_M]$ is negative.

Note the use of K_{AB} instead of K in Problem 1. It is to signify that we do not need a common gain K for all $(A, B) \in \mathcal{L}$. Perhaps we can have separate gains K_{AB} for every $(A, B) \in \mathcal{L}$ satisfying Problem 1 and the RGS strategy described in Section IV-A will search for it. However the optimization problem described in Problem 1 is semi-infinite¹⁴ and is hence not computationally tractable. We will now pose *Problem 1* as a finite optimization problem.

We can always bound the compact set \mathcal{L} by a convex polytope. Define a polytope¹⁵ $\mathcal{P} = \text{Conv}\{\mathcal{V}\}$ where $\mathcal{V} = \{(A_i, B_i) : i = 1, 2, \dots, m\}$, the m vertices of the convex polytope s.t., if $(A, B) \in \mathcal{L}$ then $(A, B) \in \mathcal{P}$. Then $\mathcal{L} \subseteq \mathcal{P}$.

We now give the following example to illustrate concepts related to \mathcal{S} , \mathcal{L} and \mathcal{P} (discussed above) and also discuss how to calculate δ_A and δ_B (discussed in *Assumption 3*).

Example 2: Consider the following scalar LTV system:

$$\dot{x}_1 = \frac{a(t)^3 c(t)^2}{b'} x_1 + \frac{\sqrt{b' c(t)}}{a(t)^{2/3}} u; \quad y = x_1 \quad (32)$$

Here a , b' , c are the physical parameters which may represent quantities like mass, friction coefficient, resistance, capacitance etc. a and c are time varying while b' is an uncertain parameter. a and c varies as: $a(t) = a^* - \frac{a^*}{2} \exp\left(-\frac{t}{\tau_a}\right)$, $c(t) = \frac{c^*}{2} + \frac{c^*}{2} \exp\left(-\frac{t}{\tau_c}\right)$ and b' lies in the uncertainty set $[b^*, \frac{3b^*}{2}]$. Here physical parameter $\Theta = [a, b, c]$ and hence $p = 3$. From the time variation of a and c we can conclude that $a \in [\frac{a^*}{2}, a^*]$ and $c \in [\frac{c^*}{2}, c^*]$. Therefore,

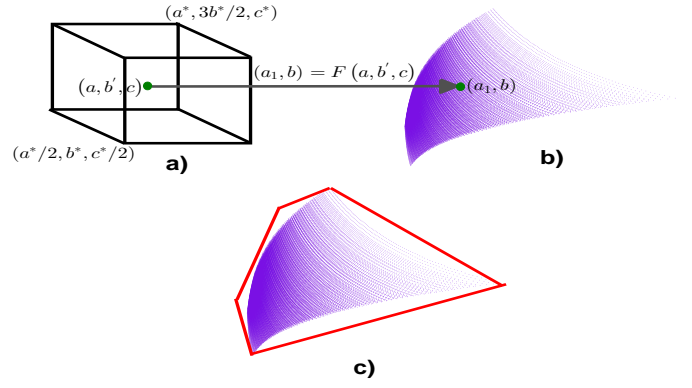


Figure 8. a) Uncertainty set \mathcal{S} associated with the physical parameters. The coordinates of two diagonally opposite vertices is shown in the figure. b) Uncertainty set \mathcal{L} associated with the LTV system characterized by equation (15). c) Bounding Convex Polytope \mathcal{P} of set \mathcal{L} . The red lines are the edges of the polytope \mathcal{P} . \mathcal{P} has 5 vertices which forms the elements of set \mathcal{V} .

$\mathcal{S} \in \left[\frac{a^*}{2}, a^*\right] \times \left[b^*, \frac{3b^*}{2}\right] \times \left[\frac{c^*}{2}, c^*\right]$ which is an hypercube as shown in Fig. 8a.

To find set \mathcal{L} first note that for this example $N = 1$ as the system described by equation (32) is scalar. Therefore $\mathcal{L} \subset \mathbb{R}^2$ and every element $[a_1, b]^T \in \mathcal{L}$ is a map $[a_1, b]^T = F(a, b', c)$ where

$$F(a, b', c) = \begin{bmatrix} \frac{a^3 c^2}{b'} \\ \frac{\sqrt{b' c}}{a^{2/3}} \end{bmatrix} \quad (33)$$

One method to obtain set \mathcal{L} is to divide the hypercube \mathcal{S} into uniform grids and then map each grid using equation (33). Set \mathcal{L} for this example is shown in Fig. 8b. Though this method to obtain \mathcal{L} from \mathcal{S} is computationally expensive, one must appreciate that for a general system there is no other elegant method. Now we want to find a convex polytope \mathcal{P} which bounds \mathcal{L} . One such polytope is shown in Fig. 8c. This polytope has $m = 5$ vertices. In practise polytope \mathcal{P} can be found using *convex-hull functions* available widely in many programming languages. One popular reference is [29].

We now discuss how to calculate δA and δB for this example. At this point one must appreciate that in most practical scenario the controller designer may not explicitly know the equations governing the rate of change of physical parameters, i.e. say in this example the designer may not know $a(t)$ and $c(t)$ explicitly. However it seems practical to assume knowledge of the bounds on the rate of change of physical parameters, i.e. controller designer may know that $0 < \dot{a} \leq \frac{a^*}{2\tau_a}$ and $-\frac{c^*}{2\tau_c} \leq \dot{c} < 0$. There is no standard way to calculate δA and δB from these bounds. Also dependent on the method used, one may get different estimate of δA and δB . For this example δA and δB is calculated as follows.

$$\begin{aligned} \delta A &= \max \left(\left| \frac{d}{dt} \left(\frac{a(t)^3 c(t)^2}{b'} \right) \right| \right) = \max \left(\frac{|3c^2 a^2 \dot{a} + 2a^3 c \dot{c}|}{b'} \right) \\ &= \frac{\max(3 \sup(c)^2 \sup(a)^2 \max(\dot{a}), 2 \sup(a)^3 \sup(c) \max(|\dot{c}|))}{\inf(b')} \\ &= \frac{\max(3(c^*)^2 (a^*)^2 \left(\frac{a^*}{2\tau_a}\right), 2(a^*)^3 (c^*) \left(\frac{c^*}{2\tau_c}\right))}{(b^*)^2} \\ &= \frac{(a^*)^3 (c^*)^2}{2(b^*)^2} \max \left(\frac{3}{\tau_a}, \frac{2}{\tau_c} \right) \end{aligned}$$

¹⁴Semi-Infinite optimization problems are the ones with infinite constraints.

¹⁵For a given \mathcal{L} , \mathcal{P} is not unique.

$$\begin{aligned}
\delta_B &= \max \left(\left| \frac{d}{dt} \left(\frac{\sqrt{b'c(t)}}{a(t)^{2/3}} \right) \right| \right) \\
&= \max \left(\left| \sqrt{b'} \left| -\frac{2\sqrt{c}\dot{a}}{3a^{5/3}} + \frac{\dot{c}}{2\sqrt{c}a^{2/3}} \right| \right| \right) \\
&= \sqrt{\sup(b')} \left(\frac{2\sqrt{\sup(c)} \left(\frac{a^*}{2\tau_a} \right)}{3 \inf(a)^{5/3}} + \frac{\left(\frac{c^*}{2\tau_c} \right)}{2\sqrt{\inf(c)} \inf(a)^{2/3}} \right) \\
&= \frac{\sqrt{c^*}}{(a^*)^{2/3}} \left(\frac{2^{5/3}}{3\tau_c} + \frac{1}{2^{5/6}\tau_c} \right)
\end{aligned}$$

Lemma 3: Under Assumption 4, if for a given $P \in \mathbb{R}^{N \times N}$ and $s \in \mathbb{R}$ there exist a $K_i \in [k_m, k_M]$ s.t.

$$(A_i - B_i K_i C)^T P + P(A_i - B_i K_i C) \preceq sI, \quad (A_i, B_i) \in \mathcal{V}$$

then there exist a $K_{AB} \in [k_m, k_M]$ s.t.

$$(A - BK_{AB}C)^T P + P(A - BK_{AB}C) \preceq sI \quad \forall (A, B) \in \mathcal{L}$$

Proof: We first define a $N \times N$ matrix Γ all elements of which are 0 except its $(N, 1)$ element which is 1. Also note that all $(A, B) \in \mathcal{L}$ can be written as a convex combination of the elements \mathcal{V} of the convex polytope \mathcal{P} . Mathematically, $\forall (A, B) \in \mathcal{L}$ there exists scalars $\theta_i \geq 0, i = 1, 2, \dots, m$ s.t.

$$(A, B) = \sum_{i=1}^m \theta_i (A_i, B_i) \quad \text{and} \quad \sum_{i=1}^m \theta_i = 1$$

where, $(A_i, B_i) \in \mathcal{V} \forall i = 1, 2, \dots, m$. Now,

$$\begin{aligned}
&(A - BK_{AB}C)^T P + P(A - BK_{AB}C) \\
&= (A^T P + PA) - bK_{AB} (\Gamma^T P + P\Gamma) \\
&= \sum_{i=1}^m \theta_i (A_i^T P + PA_i) - (\Gamma^T P + P\Gamma) K_{AB} \sum_{i=1}^m \theta_i b_i \quad (34)
\end{aligned}$$

Equation (34) is possible because $BC = b(t)\Gamma$ owing to the special structure of B and C matrix. Using the inequality

$$(A_i - B_i K_i C)^T P + P(A_i - B_i K_i C) \preceq sI, \quad (A_i, B_i) \in \mathcal{V}$$

in equation (34) we have

$$\begin{aligned}
&(A - BK_{AB}C)^T P + P(A - BK_{AB}C) \\
&\preceq \left[\sum_{i=1}^m \theta_i K_i b_i - K_{AB} \sum_{i=1}^m \theta_i b_i \right] (\Gamma^T P + P\Gamma) + sI \quad (35)
\end{aligned}$$

Choosing, $K_{AB} = \frac{\sum_{i=1}^m \theta_i K_i b_i}{\sum_{i=1}^m \theta_i b_i}$ in inequality (35) yields

$$(A - BK_{AB}C)^T P + P(A - BK_{AB}C) \preceq sI$$

Now all we need to do is to prove that the chosen K_{AB} lies in the interval $[k_m, k_M]$. We know that $k_m \leq K_i \leq k_M$. Therefore under Assumption 4¹⁶,

$$\begin{aligned}
\frac{\sum_{i=1}^m \theta_i k_m b_i}{\sum_{i=1}^m \theta_i b_i} &\leq K_{AB} \leq \frac{\sum_{i=1}^m \theta_i k_M b_i}{\sum_{i=1}^m \theta_i b_i} \Rightarrow k_m \leq K_{AB} \leq k_M
\end{aligned}$$

This concludes the proof of Lemma 3. The importance of Lemma 3 is that it reduces the semi-infinite optimization problem posed in Problem 1 into a finite optimization problem. This results into the most important result of this section.

Theorem 2: [C1] holds if the optimal value of the problem minimize: s

subject to:

$$(A_i - B_i K_i C)^T P + P(A_i - B_i K_i C) \preceq sI \quad \forall (A_i, B_i) \in \mathcal{V}$$

$$k_m \leq K_i \leq k_M, \quad i = 1, 2, \dots, m$$

$$P \succ 0$$

with design variables $s \in \mathbb{R}, P \in \mathbb{R}^{N \times N}$ and $K_i \in \mathbb{R}, i = 1, 2, \dots, m$ is negative.

Proof: The proof follows from Problem 1 and Lemma 3.

Note that while Problem 1 is a *necessary and sufficient* condition, Theorem 2 is a *sufficient* condition. This is due to the fact that $\mathcal{L} \subseteq \mathcal{P}$ leading to some conservativeness in the optimization problem proposed in Theorem 2.

Theorem 2 poses the classical *BMI Eigenvalue Minimization Problem (BMI-EMP)* in variables P and K_i . As such BMI's are non-convex in nature leading to multiple local minimas. Several algorithms to find the local minima exist in literature (see [30], [31]). Algorithms for global minimization of BMI's is rather rare and have received attention in works like [32], [33]. Our approach is similar to [32] which is basically a *Branch and Bound* algorithm. Such an algorithm works by bounding s by a lower bound Φ_L and an upper bound Φ_U , i.e. $\Phi_L \leq s \leq \Phi_U$. The algorithm then progressively refines the search to reduce $\Phi_U - \Phi_L$. Our main algorithm consists of *Algorithm 4.1* of [32] (Page 4). The *Alternating SDP method* mentioned in [34] (Page 2) is used for calculating Φ_U . For calculating Φ_L we have used the *convex relaxation* technique first introduced in [33] (also discussed in [34], equation (9)). In Appendix B we present a working knowledge of our algorithm. For detailed explanation the readers may refer the corresponding work [32], [34].

Theorem 2 poses an optimization problem with $(A_i, B_i) \in \mathcal{V}, k_m$ and k_M as inputs and P, s and $K_i, i = 1, 2, \dots, m$ as outputs. But k_m and k_M are not known. An initial estimate of $k_m = k_m^{RH}$ and $k_M = k_M^{RH}$ is obtained by using Routh-Hurwitz criteria¹⁷ for each $(A_i, B_i) \in \mathcal{V}$. Let $K_i = K_i^{RH}, i = 1, 2, \dots, m$ be the output of the optimization problem with this initial estimate. Let $k_m^* = \min_{1 \leq i \leq m} (K_i^{RH})$ and $k_M^* = \max_{1 \leq i \leq m} (K_i^{RH})$, then the following holds:

1) $k_m^* \geq k_m^{RH}$ and $k_M^* \leq k_M^{RH}$. This is because $k_m^{RH} \leq K_i^{RH} \leq k_M^{RH}, \forall i = 1, 2, \dots, m$ and hence

$$k_m^{RH} \leq \min_{1 \leq i \leq m} (K_i^{RH}) \leq \max_{1 \leq i \leq m} (K_i^{RH}) \leq k_M^{RH}$$

¹⁷Routh-Hurwitz criteria is used to find the bounds on the feedback gains for which a SISO LTI system is closed loop stable. Refer [35] for details.

¹⁶Without Assumption 4, the denominator $\sum_{i=1}^m \theta_i b_i$ may become 0.

2) The outputs, P , s and K_i , obtained by running the optimization algorithm with a) $k_m = k_m^{RH}$ and $k_M = k_M^{RH}$ or b) $k_m = k_m^*$ and $k_M = k_M^*$, will be the same. This is because the gains K_i^{RH} obtained by running the optimization algorithm with $k_m = k_m^{RH}$ and $k_M = k_M^{RH}$ also satisfies the bounds $k_m^* \leq K_i^{RH} \leq k_M^*$.

Therefore if we choose $k_m = k_m^*$ and $k_M = k_M^*$ we would get a smaller RGS gain set, i.e. $(k_M^* - k_m^*) \leq (k_M^{RH} - k_m^{RH})$, without compromising the convergence coefficient s . A smaller RGS gain set will ease the controller design in an analog setting.

We now give a bound on $\lambda_M^{\mathcal{L}}$ (defined in *Theorem 1*). It is not possible to calculate $\lambda_M^{\mathcal{L}}$ with the formula given in *Theorem 1* as it will involve search over the dense set $S_Q^{\mathcal{L}}$. Define a set

$$S_Q^{\mathcal{P}} = \left\{ Q : Q = (A - BKC)^T P + P(A - BKC) \right. \\ \left. (A, B) \in \mathcal{P}, K \in [k_m, k_M] \right\}$$

Let $\lambda_M^{\mathcal{P}} = \max_{Q \in S_Q^{\mathcal{P}}} \lambda_M(Q)$. As $\mathcal{L} \subseteq \mathcal{P}$ it is obvious that, $S_Q^{\mathcal{L}} \subseteq S_Q^{\mathcal{P}}$ ($S_Q^{\mathcal{L}}$ defined in *Theorem 1*). Therefore¹⁸, $\lambda_M^{\mathcal{L}} \leq \lambda_M^{\mathcal{P}}$. Thus $\lambda_M^{\mathcal{P}}$ gives an estimate of $\lambda_M^{\mathcal{L}}$ by upper bounding it. It can be shown that for a scalar gain K and the specific structure of B and C (refer equation (15)), it can be proved that $S_Q^{\mathcal{P}}$ is compact convex set. Also $\lambda_M(Q)$ is a convex function for all $Q \in \mathbf{S}^+$ (refer Page 82 of [36]). It is well known that global maxima of a convex function over a convex compact set only occurs at some extreme points of the set (refer [37]). Thus the problem of maximizing $\lambda_M(\cdot)$ over $Q \in S_Q^{\mathcal{P}}$ reduces to maximizing $\lambda_M(\cdot)$ over $Q \in S_Q^{\mathcal{V}}$ where

$$S_Q^{\mathcal{V}} = \left\{ Q : Q = (A - BKC)^T P + P(A - BKC) \right. \\ \left. (A, B) \in \mathcal{V}, K \in \{k_m, k_M\} \right\}$$

the set of vertices of $S_Q^{\mathcal{P}}$. This leads to the following formula

$$\lambda_M^{\mathcal{L}} \leq \lambda_M^{\mathcal{P}} = \max_{Q \in S_Q^{\mathcal{V}}} \lambda_M(Q) \quad (36)$$

Inequality (36) can be used to obtain an estimate of $\lambda_M^{\mathcal{L}}$.

Remark 8: As mentioned in the beginning of Section IV, for a controller to be implementable in analog framework it has to be simple. Though the synthesis of RGS parameters ($k_m, k_M, T, \alpha, \gamma$ and P) is complex, one must appreciate that designing a controller is a 'one time deal'. RGS in itself is a simple gain-scheduled controller governed by equation (16).

V. EXAMPLE

Parallel Plate Electrostatic Actuator (PPA) shown in Fig. 9a forms a vital component of several miniaturized systems. We perform regulatory control of PPA to show effectiveness of the proposed analog architecture and RGS strategy. PPA's as described in [20] (page 183) follows the following dynamics

$$m\ddot{y} + b\dot{y} + ky = \frac{\varepsilon A}{2(G-y)^2} V_s^2 \quad (37)$$

¹⁸This is more like saying that the maximum of a function ($\lambda_M(\cdot)$ here) over a bigger set ($S_Q^{\mathcal{P}}$ here) will be greater than the maximum over a smaller set ($S_Q^{\mathcal{L}}$ here).

which is nonlinear in nature. Plant parameter includes spring constant κ , damping coefficient b , moving plate mass and area m and A respectively, permittivity ε and maximum plate gap G . As we are interested in only regulatory control, we use the following linearized model

$$\begin{bmatrix} \dot{x}_1 \\ \dot{x}_2 \end{bmatrix} = \begin{bmatrix} 0 & 1 \\ -\frac{\kappa(G-3G_o)}{m(G-G_o)} & -\frac{b}{m} \end{bmatrix} \begin{bmatrix} x_1 \\ x_2 \end{bmatrix} + \begin{bmatrix} 0 \\ \frac{\sqrt{2\varepsilon A \kappa G_o}}{m(G-G_o)} \end{bmatrix} u_r \quad (38)$$

where, x_1 is the displacement from the operating point G_o . Plant output is the moving plate position $y = G_o + x_1$. Plant input is $V_s = V_b + V_u$. Comparing with RGS theory, $V_b = u_b$, the bias voltage to maintain G_o as the operating point and $V_u = u_r = KV_e = K(G_o - y) = -Kx_1$, the regulation voltage supplied by the Memristive AGC. Plant parameter includes spring constant κ , damping coefficient b , moving plate mass and area m and A respectively, permittivity ε and maximum plate gap G . For $G_o > \frac{G}{3}$, the system has an unstable pole. We perform regulation around $G_o = \frac{2G}{3}$.

The *true* plant parameters are, $m = 3 \times 10^{-3} \text{ kg}$, $b = 1.79 \times 10^{-2} \text{ Nsm}^{-1}$, $G = 10^{-3} \text{ m}$, $A = 1.6 \times 10^{-3} \text{ m}^2$. G and A are uncertain but lie in the set $G \in \mathcal{S}_G = [0.5 \ 2.0] \times 10^{-3} \text{ m}$, $A \in \mathcal{S}_A = [1.2 \ 1.8] \times 10^{-3} \text{ m}^2$. ε varies due to surrounding condition as $\varepsilon(t) = 5\varepsilon_o + 1.5\varepsilon_o \sin(7.854t)$ where ε_o is the permittivity of vacuum. Spring loosening causes κ to decrease as $\kappa(t) = 0.08 + 0.087e^{-0.8t} \text{ Nm}^{-1}$. Now we will discuss the steps involved in implementing RGS in an analog framework.

Step 1 (Identify \mathcal{S}): \mathcal{S} is the uncertainty set of physical parameters first defined in Page 8. Define set $\mathcal{S}_\varepsilon = [3.5\varepsilon_o \ 6.5\varepsilon_o]$ and $\mathcal{S}_\kappa = [0.08 \ 0.167] \text{ Nm}^{-1}$. Then the ordered pair $(G, A, \varepsilon, \kappa) \in \mathcal{S} = \mathcal{S}_G \times \mathcal{S}_A \times \mathcal{S}_\varepsilon \times \mathcal{S}_\kappa$. Note that here $p = 4$. **Step 2** (Find \mathcal{P}): To do this we numerically map \mathcal{S} to \mathcal{L} (as shown in *Example 2*) and then use *convhulln* function of MATLAB to find a convex polytope \mathcal{P} s.t. $\mathcal{L} \subseteq \mathcal{P}$. In this case \mathcal{P} consist of $m = 4$ vertices. We explicitly don't mention the computed \mathcal{P} for the sake of neatness.

Step 3 (Compute P, s, α, k_m, k_M): Solving optimization problem proposed in *Theorem 2* we get, $s = 0.917$, $k_m = 8600$ and $k_M = 86000$ and $P = \begin{bmatrix} 0.9937 & 0.0757 \\ 0.0757 & 0.0895 \end{bmatrix}$. Here, $\lambda_M(P) = 1$, hence $\alpha = \frac{s}{\lambda_M(P)} = 0.917$.

Step 4 (Compute $\lambda_m(P), \lambda_M^{\mathcal{L}}, \delta$): For the calculated P , $\lambda_m(P) = 0.083$. From equation (36), $\lambda_M^{\mathcal{L}} = 29.1$. We will now calculate δ_A and δ_B for this example. As mentioned in *Example 2* the controller designer does not know $\kappa(t)$ and $\varepsilon(t)$ explicitly but they do know the bounds on $\dot{\kappa}$ and $\dot{\varepsilon}$ which for this example is: $(-0.087 \times 0.8) \leq \dot{\kappa} < 0$ and $-(1.5 \times 7.854 \times \varepsilon_o) \leq \dot{\varepsilon} \leq (1.5 \times 7.854 \times \varepsilon_o)$.

First note that (2×2) element of the system matrix of the linearized PPA model (described by equation (38)) is not time varying. Hence δ_A can be simply written as

$$\begin{aligned} \delta_A &= \max \left(\left| \frac{d}{dt} \left(-\frac{\kappa(t)(G-3G_o)}{m(G-G_o)} \right) \right| \right) \\ &= \max \left(\left| \frac{d}{dt} \left(-\frac{\kappa(t)(G-3(\frac{2G}{3}))}{m(G-\frac{2G}{3})} \right) \right| \right) \\ &= \frac{3 \max(|\dot{\kappa}|)}{m} \end{aligned}$$

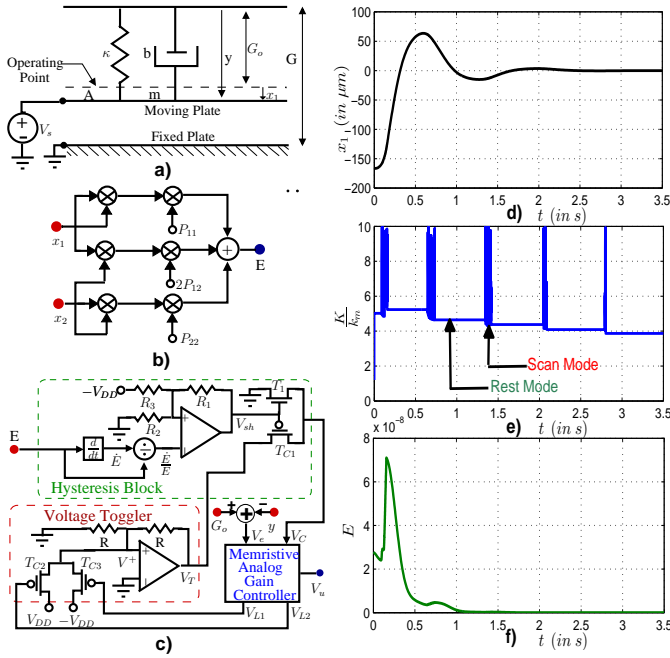


Figure 9. a) Schematic of PPA. b) Analog Implementation of $E = x^T P x$ for $P \in \mathbb{R}^{2 \times 2}$. Note that, $P_{12} = P_{21}$ as $P \in \mathbf{S}$. c) Analog Implementation of RGS. d), e), f) Plots of plate position error x_1 (from operating point G_o), normalized RGS gain $\frac{K}{k_m}$ and Lyapunov Function $E = x^T P x$ with respect to time.

$$\begin{aligned}
 \delta_B &= \max \left(\left| \frac{d}{dt} \left(\frac{\sqrt{2\varepsilon(t)A\kappa(t)G_o}}{m(G-G_o)} \right) \right| \right) \\
 &= \max \left(\left| \frac{d}{dt} \left(\frac{\sqrt{2\varepsilon(t)A\kappa(t)\left(\frac{2G}{3}\right)}}{m\left(G-\frac{2G}{3}\right)} \right) \right| \right) \\
 &= \frac{1}{m} \sqrt{\frac{12 \sup(S_A)}{\inf(S_G)}} \max \left(\left| \sqrt{\varepsilon \dot{K}} \right| \right) \\
 &= \frac{1}{m} \sqrt{\frac{12 \sup(S_A)}{\inf(S_G)}} \max \left(\left| \frac{\kappa \dot{\varepsilon} + \varepsilon \dot{\kappa}}{2\sqrt{\varepsilon}\sqrt{\kappa}} \right| \right) \\
 &= \frac{1}{m} \sqrt{\frac{12 \sup(S_A)}{\inf(S_G)}} \left(\frac{\sup(S_\kappa) \max(|\dot{\varepsilon}|) + \sup(S_\varepsilon) \max(|\dot{\kappa}|)}{2\sqrt{\inf(S_\varepsilon)}\sqrt{\inf(S_\kappa)}} \right)
 \end{aligned}$$

Substituting the values in the above equation of δ_A and δ_B we get $\delta = \delta_A + k_M \delta_B = 1351$.

Step 5 (Compute T and γ): We arbitrarily choose $\gamma = 0.5$. Substituting $\gamma = 0.5$ in inequality (29) we get $T < 1.66 \times 10^{-7} s$. Hence we choose $T = 10^{-7} s$.

Step 6 (Analog Design): Fig. 9b and 9c combined shows the analog implementation of RGS. The error voltage V_e is the plate position error, i.e. $V_e = -x_1 = (G_o - y)$. The gain control voltage V_C is controlled by the Hysteresis Block and the Voltage Toggler block. In Rest Mode $V_C = 0$ thereby ensuring that the gain \mathcal{M} is constant (refer equation (12)). In Scan Mode $V_C \in \{-V_{DD}, V_{DD}\}$, $V_C = V_{DD}$ to scan from R_{off}^S to R_{on}^S and $V_C = -V_{DD}$ to scan from R_{on}^S to R_{off}^S (refer equation (12)). R_C controls \dot{M} , the rate of change of gain (refer equation (12)). Setting $R_C = \frac{V_{DD} T}{Q_M^S}$ ensures a scan time of T . The derivation of R_C is simple. Note that the resistance of memristor will change from R_{off}^S to R_{on}^S if we pass a charge Q_M^S through it. We want this change to happen in time T and hence the desired current is $\frac{Q_M^S}{T}$. As $V_C = V_{DD}$ in scan mode, the required resistance $R_C = \frac{V_{DD}}{\left(\frac{Q_M^S}{T}\right)} = \frac{V_{DD} T}{Q_M^S}$.

The Hysteresis Block is a conventional inverting schmitt trigger. Tuning $R_1 = \frac{2(V_{DD}-\alpha)}{\alpha(1-\gamma)} R_2$ and $R_3 = \frac{2(V_{DD}-\alpha)}{\alpha(1+\gamma)} R_2$ ensures¹⁹ that the schmitt trigger's output goes from V_{DD} to $-V_{DD}$ at $\frac{\dot{E}}{E} = -\gamma\alpha$ and from $-V_{DD}$ to V_{DD} at $\frac{\dot{E}}{E} = -\alpha$. Due to the transistor arrangement in Hysteresis Block: 1) $V_C = 0$ when $V_{sh} = V_{DD}$. Therefore $V_{sh} = V_{DD}$ implies Rest Mode. 2) $V_C = V_T$ when $V_{sh} = -V_{DD}$. It will be explained next that $V_T \in \{-V_{DD}, V_{DD}\}$. Therefore $V_{sh} = -V_{DD}$ implies Scan Mode. So we can conclude that the Hysteresis Block goes from Rest Mode to Scan Mode when $\frac{\dot{E}}{E} = -\gamma\alpha$ and from Scan Mode to Rest Mode when $\frac{\dot{E}}{E} = -\alpha$. This is in accordance with the hysteresis shown in Fig. 6a.

V_T , the output of the Voltage Toggler block, toggles between $-V_{DD}$ and V_{DD} . Recalling equation (12), this will result in the gain of the memristive gain control block reflect between $\left[\frac{R_{on}^S}{R_I}, \frac{R_{off}^S}{R_I} \right]$. We now explain the working of this block. Say $V_T = V_{DD}$ and the zone indicating voltages (refer Fig. 3) $V_{L1} = V_{L2} = V_{DD}$. As $V_{L1} = V_{L2} = V_{DD}$, transistors T_{C2} and T_{C3} are *OFF*. The voltage $V^+ = \frac{V_T}{2} = \frac{V_{DD}}{2}$. Since $V^+ = \frac{V_{DD}}{2} > 0$, $V_T = V_{DD}$. This shows that the output of Voltage Toggler block is stable. As $V_T = V_{DD}$, memristor's resistance M will decrease till $M = R_{on}^S$ (see equation (12)) at which point $V_{L1} = -V_{DD}$ and $V_{L2} = V_{DD}$ (refer Case 2 of III-D). T_{C3} will be momentarily *ON* making $V^+ = -V_{DD}$ and hence driving V_T to $-V_{DD}$. Then M will increase from R_{on}^S , making $V_{L1} = V_{L2} = V_{DD}$ and hence driving T_{C3} to *OFF* state. When this occurs $V^+ = \frac{V_T}{2} = -\frac{V_{DD}}{2}$. As $V^+ = -\frac{V_{DD}}{2} < 0$, $V_T = -V_{DD}$. Similar momentary transition of T_{C2} to *ON* state will toggle V_T from $-V_{DD}$ to V_{DD} when $M = R_{off}^S$.

Several plots corresponding the regulatory performance of PPA under RGS control strategy is shown in Fig. 9d, e, f. It is interesting to observe that an LTV system can have multiple rest-scan cycle (see Fig. 9e). This is because for a time varying system a *stabilizing gain* at a given instant may not be the *stabilizing gain* at a later instant due to the change in system dynamics. Unlike LTV system, a LTI system will have only 1 rest-scan cycle.

Remark 9: In this example T is very low which may seem to challenge analog design. However for all practical purposes it is not so. For the sake of simulation we choose a fictitious time variation of $\kappa(t)$ and $\varepsilon(t)$ which is quite fast compared to that found in nature. Therefore δ_A and δ_B is high (refer **Step 4**) resulting in a high δ and hence a low scan time T (refer inequality (29)). In practice, time variation of a system caused by ageing effect and atmospheric variation is a slow process. Hence, T will be much higher.

Remark 10: To control an array of miniaturized devices (say PPA) one can reduce the circuitry required by identifying the components of the circuit which can be common for the entire array. For example, Synchronization Block can be common for the entire array. Synchronization of each pair of coupled Memristor Gain Block and Integrator (refer Fig. 3) can be done in a time multiplexed manner, i.e. each pair of coupled Memristor Gain Block and Integrator is synchronized using

¹⁹The designer is free to choose the resistance R_2 .

one Synchronization Block. The oscillator shown in the circuit of Fig. 3 can also be common for the entire array.

VI. DISCUSSION

To the best of authors knowledge this paper is one of the first attempts towards understanding the use of memristor in control applications. A memristive variable gain architecture has been proposed. We then propose (and prove) RGS control strategy which can be implemented using this framework. Simplicity of RGS control strategy is demonstrated using an example. The extension of this work can take two course.

From *Circuit Standpoint* one may try to design an analog circuit which mimics the circuit shown in Fig. 2 but with a *lesser number of op-amps*. Since the synthesis of memristor is still an engineering challenge, one may speculate regarding the use of variable CMOS resistors (refer [21]) to implement the analog gain controller proposed in Section III.

Two milestones have to be addressed before RGS is practically feasible: 1) RGS needs information about the states x which is obtained by differentiating the output y $N-1$ times. But differentiation might amplify the noise. 2) RGS relies on the knowledge of E which is obtained by performing $x^T P x$ using analog circuitry. Such analog implementation will be easier if P is sparse. Hence from *Control Theoretic Standpoint*, addressing these two issues will be the first target of the authors. Later point has been addressed in [38]. Extending RGS to SISO non-linear and in general MIMO systems would be the next step. It would also be interesting to explore other simple control strategies (like [39]) which can be implemented in analog framework.

APPENDIX A

PROOF OF LEMMA 1: DRIFTING NATURE OF STABILIZING GAIN SET $\mathcal{K}_{P,s}(t)$

To prove *Lemma 1* we will take the following steps:

- 1) Pick a gain $K \in \mathcal{K}_{P,s}(t)$.
- 2) Prove that if $\delta t \rightarrow 0$ then there exist a $\Delta K \rightarrow 0$ s.t. $(K + \Delta K) \in \mathcal{K}_{P,s}(t + \delta t)$.
- 3) As $\Delta K \rightarrow 0$, $(K + \Delta K) \in \mathcal{K}_{P,s}(t)$. Hence the gain $K + \Delta K$ belongs to both the sets, $\mathcal{K}_{P,s}(t)$ and $\mathcal{K}_{P,s}(t + \delta t)$. This implies that $\mathcal{K}_{P,s}(t) \cap \mathcal{K}_{P,s}(t + \delta t) \neq \emptyset$.

Now we proceed with the proof. We first pick a gain $K \in \mathcal{K}_{P,s}(t)$. As $\mathcal{K}_{P,s}(t) \neq \emptyset$, $\forall t \geq 0$ such a gain will exist. For a time $t = t^*$ there exists a gain $K^* \in \mathcal{K}_{P,s}(t^*)$ and a scalar $s^* > s$ s.t. the following equality holds

$$(A^* - B^* K^* C)^T P + P (A^* - B^* K^* C) = -s^* I \quad (39)$$

In equation (39) $A^* = A(t^*)$ and $B^* = B(t^*)$. Equation (38) directly follows from the very definition of stabilizing gain set (defined in page 7). Lets say that at time $t = t^* + \delta t$ there exist a $K^* + \Delta K$ s.t.

$$\begin{aligned} & [(A^* + \delta A) - (B^* + \delta B)(K^* + \Delta K)C]^T P \\ & + P [(A^* + \delta A) - (B^* + \delta B)(K^* + \Delta K)C] = -s^* I \end{aligned} \quad (40)$$

In equation (40) $\delta A = \dot{A}(t^*) \delta t$ and $\delta B = \dot{B}(t^*) \delta t$ are infinitesimal change in A and B respectively. Note that ΔK is a scalar. Hence, substituting equation (39) in (40) yields

$$\Delta K \mathcal{R} = (\delta A - \delta B K^* C)^T P + P (\delta A - \delta B K^* C) \quad (41)$$

where, $\mathcal{R} = C^T (B^* + \delta B)^T P + P (B^* + \delta B) C$. Hence if ΔK satisfies equation (41) then $K^* + \Delta K \in \mathcal{K}_{P,s}(t^* + \delta t)$. Now all we need to do is to prove that ΔK is infinitesimal, i.e. $\Delta K \rightarrow 0$ if $\delta A \rightarrow 0$ and $\delta B \rightarrow 0$. Taking norm on both side of equation (41) we get,

$$\begin{aligned} \Delta K \|\mathcal{R}\| & \leq 2 \|P\| (\|\delta A\| + K^* \|\delta B\| \|C\|) \\ \Delta K & \leq \frac{2 \|P\| (\delta A + K^* \delta B)}{\|\mathcal{R}\|} \delta t \end{aligned} \quad (42)$$

Since $\|\mathcal{R}\|$ is finite it is obvious from inequality (42) that $\Delta K \rightarrow 0$ as $\delta t \rightarrow 0$. This concludes the proof.

APPENDIX B

GLOBAL SOLUTION OF BMI-EMP

Theorem 2 involves solving the following BMI-EMP optimization problem

OP1:

minimize: s

subject to:

$$\begin{aligned} & (A_i - B_i K_i C)^T P + P (A_i - B_i K_i C) \preceq s I \quad \forall (A_i, B_i) \in \mathcal{V} \\ & k_m \leq K_i \leq k_M, \quad i = 1, 2, \dots, m \\ & P \succ 0 \end{aligned}$$

We will first justify why **OP1** is called BMI-EMP. Consider a matrix inequality of type

$$(A - BKC)^T P + P (A - BKC) \preceq s I \quad (43)$$

Given a set of A, B, C, K and P , the least possible value of s which will satisfy inequality (43) is indeed the largest eigen value of the matrix $(A - BKC)^T P + P (A - BKC)$. So if we exclude the inequalities $k_m \leq K_i \leq k_M$ and $P \succ 0$, then **OP1** can be equally casted as

$$\min_{P, K_i} \max_{(A_i, B_i) \in \mathcal{V}} \lambda_M \left((A_i - B_i K_i C)^T P + P (A_i - B_i K_i C) \right)$$

which is basically a Largest Eigenvalue Minimization Problem or just ‘‘EMP’’. Now consider the function

$$\Lambda(P, K) = \lambda_M \left((A - BKC)^T P + P (A - BKC) \right)$$

The matrix $Q(P, K) := (A - BKC)^T P + P (A - BKC)$ is *Bilinear* in the sense that it is linear in K if P is fixed and linear in P if K is fixed. As $Q \in \mathbf{S}$, the function $\Lambda(P, K) = \lambda_M(Q(P, K))$ is convex in K if P is fixed and convex in P if K is fixed.

We are interested in the global solution of BMI-EMP as a smaller value s will ensure better convergence of the LTV/LTI system. In the following we will provide a sketch of the work done in [32], [34], [33] which will be just enough to design an algorithm for global solution of BMI-EMP. However we don't provide detailed explanation of the algorithm for which the reader may refer [32].

Before proceeding forward we would like to cast **OP1** in a form which can be handled by a numerical solver. Observe that

the third constrain of **OP1** is a strict inequality which demands that the Lyapunov Matrix P has to be positive definite (*not* positive semi-definite). Such a strict inequality will impose numerical challenge and hence we replace it with the non-strict inequality $P \succeq \mu_p I$ where, $0 < \mu_p \ll 1$. Without any loss of generality: 1) We constrain the $\|P\| \leq 1$ by imposing the constrain $P \preceq I$. 2) We normalize the RGS gain set. We get the following optimization problem,

OP2:

minimize: s

subject to:

$$A_i^T P + P A_i - (B_i C)^T K_i P - K_i P (B_i C) \preceq s I \quad \forall (A_i, B_i) \in \mathcal{V}$$

$$\mu_k \leq K_i \leq 1, \quad i = 1, 2, \dots, m$$

$$\mu_p I \preceq P \preceq I$$

In the above problem, $\mu_k = \frac{k_m}{k_M} < 1$. We also redefine C as $C := [k_M \ \dots \ 0 \ 0]$, to neutralize the effect of normalizing RGS gain set.

We now define two vectors: $\mathbf{P} = [p_1 \ p_2 \ \dots \ p_{n_p}]^T$ containing the $n_p = \frac{N(N+1)}{2}$ distinct elements of symmetric matrix P and $\mathbf{K} = [K_1 \ K_2 \ \dots \ K_m]^T$ the m normalized RGS Gains of **OP2**. We also define two sets \mathcal{X}_P and \mathcal{X}_K as follows

$$\mathcal{X}_P := [-1, 1]^{n_p}; \quad \mathcal{X}_K := [\mu_k, 1]^m$$

Note that \mathcal{X}_P is a n_p dimensional unit hypercube such that²⁰ $\mathbf{P} \in \mathcal{X}_P$ and \mathcal{X}_K is a m dimensional hyper-rectangle such that $\mathbf{K} \in \mathcal{X}_K$. We also define smaller hyper-rectangle's $\mathcal{Q}_P \subseteq \mathcal{X}_P$, $\mathcal{Q}_K \subseteq \mathcal{X}_K$ and $\mathcal{Q} \subseteq \mathcal{X}_P \times \mathcal{X}_K$ as follows

$$\mathcal{Q}_P := [L_P^1, U_P^1] \times [L_P^2, U_P^2] \times \dots \times [L_P^{n_p}, U_P^{n_p}]$$

$$\mathcal{Q}_K := [L_K^1, U_K^1] \times [L_K^2, U_K^2] \times \dots \times [L_K^m, U_K^m]$$

$$\mathcal{Q} := \mathcal{Q}_P \times \mathcal{Q}_K$$

Obviously $-1 \leq L_P^i \leq U_P^i \leq 1$ and $\mu_k \leq L_K^i \leq U_K^i \leq 1$. Consider the following ‘‘constrained version’’ of **OP2** where (\mathbf{P}, \mathbf{K}) is only defined in the small hyper-rectangle \mathcal{Q} .

OP3:

minimize: s

subject to:

$$A_i^T P + P A_i - (B_i C)^T K_i P - K_i P (B_i C) \preceq s I \quad \forall (A_i, B_i) \in \mathcal{V}$$

$$\mu_k \leq K_i \leq 1, \quad i = 1, 2, \dots, m$$

$$\mu_p I \preceq P \preceq I$$

$$(\mathbf{P}, \mathbf{K}) \in \mathcal{Q}$$

The input to **OP3** is the set \mathcal{Q} and its output is $s^*(\mathcal{Q})$ which is a function of \mathcal{Q} . We want to bound $s^*(\mathcal{Q})$ by an upper and a lower bound as follows:

$$\Phi_L(\mathcal{Q}) \leq s^*(\mathcal{Q}) \leq \Phi_U(\mathcal{Q}) \quad (44)$$

The *convex relaxation* technique introduced in [33] (also discussed in [34], equation (9)) has been used to get the lower bound $\Phi_L(\mathcal{Q})$. We replace the nonlinearity $K_i P$ with a new matrix W_i . As W_i is a symmetric matrix matrix of order N we can represent it by a vector $\mathbf{W}_i = [w_{1i} \ w_{2i} \ \dots \ w_{n_p i}]^T$ containing the n_p

²⁰All the element of the Lyapunov Matrix P will be in the range $[-1, 1]$ as $P \preceq I$ according to **OP2**.

Algorithm 1 Alternating SDP Method

1. Set $\mathbf{K}^{(0)} = \text{Centroid of } \mathcal{Q}_K. (s^{(0)}, \mathbf{P}^{(0)}) = \text{OP3}(\mathcal{Q}, \mathbf{K}^{(0)})$.
 2. *if* $(s^{(0)} = \infty)$
 3. *return* ∞ .
 4. *else*
 5. Set $\delta > 0$ and $k = 0$.
 6. *do* {
 7. $(s^{(k+1)}, \mathbf{P}^{(k+1)}) = \text{OP3}(\mathcal{Q}, \mathbf{K}^{(k)})$
 8. $(s^{(k+1)}, \mathbf{K}^{(k+1)}) = \text{OP3}(\mathcal{Q}, \mathbf{P}^{(k+1)})$
 9. $k = k + 1$.
 10. } *while* $(s^{(k-1)} - s^{(k)} < \delta |s^{(k)}|)$
 11. *return* $s^{(k)}$.
 12. *end*
-

distinct elements of W_i . We now define a matrix $\mathbf{W} = [\mathbf{W}_1^T \ \mathbf{W}_2^T \ \dots \ \mathbf{W}_m^T]^T$. If **OP3** is expanded in terms of p_j and K_i then the element w_{ji} of \mathbf{W} is constrained by the equality $w_{ji} = K_i p_j$. Rather than imposing this equality constrain we let w_{ji} to be a free variable which can take any value in the set $\mathcal{W}(\mathcal{Q})$ defined as

$$\mathcal{W}(\mathcal{Q}) := \left\{ \mathbf{W} \left| \begin{array}{l} (\mathbf{P}, \mathbf{K}) \in \mathcal{Q} \\ w_{ji} \geq L_K^i p_j + L_P^j K_i - L_K^i L_P^j \\ w_{ji} \geq U_K^i p_j + U_P^j K_i - U_K^i U_P^j \\ w_{ji} \leq U_K^i p_j + L_P^j K_i - U_K^i L_P^j \\ w_{ji} \leq L_K^i p_j + U_P^j K_i - L_K^i U_P^j \end{array} \right. \right\}$$

By performing the convex relaxation stated above we get the following optimization problem.

OP4:

minimize: s

subject to:

$$A_i^T P + P A_i - (B_i C)^T W_i - W_i (B_i C) \preceq s I \quad \forall (A_i, B_i) \in \mathcal{V}$$

$$\mu_p I \preceq P \preceq I$$

$$\mu_p K_i I \mu_k \preceq W_i \preceq K_i I, \quad i = 1, 2, \dots, m$$

$$(\mathbf{P}, \mathbf{K}) \in \mathcal{Q}$$

$$\mathbf{W} \in \mathcal{W}(\mathcal{Q})$$

The input to **OP4** is the set \mathcal{Q} and its output is $\Phi_L(\mathcal{Q})$. As **OP4** is a relaxed version of **OP3**, $\Phi_L(\mathcal{Q}) \leq s^*(\mathcal{Q})$. Note that **OP4** is a convex optimization problem, more specifically a *Semi-Definite Program(SDP)* which can be solved by numerical solvers like CVX[40].

We now concentrate on defining the upper bound $\Phi_U(\mathcal{Q})$. Any local minima of **OP3** can indeed be the upper bound $\Phi_U(\mathcal{Q})$. We use the *Alternating SDP Method* discussed in [33], [41]. Alternating SDP method relies on the Bi-Convex nature of **OP3**, i.e. **OP3** becomes a convex problem (more specifically SDP) in \mathbf{P} with \mathbf{K} fixed or a convex problem in \mathbf{K} with \mathbf{P} fixed. Alternating SDP Method is summarized in *Algorithm 1*. We represent by **OP3**(\mathcal{Q}, \mathbf{K}') the optimization problem obtained by fixing $\mathbf{K} = \mathbf{K}'$ in **OP3** and **OP3**(\mathcal{Q}, \mathbf{P}') the optimization problem obtained by fixing $\mathbf{P} = \mathbf{P}'$ in **OP3**. The input to **OP3**(\mathcal{Q}, \mathbf{K}') is the small hyper-rectangle \mathcal{Q} and the fixed RGS gain \mathbf{K}' while the input to **OP3**(\mathcal{Q}, \mathbf{P}') is the small hyper-rectangle \mathcal{Q} and the fixed Lyapunov Matrix \mathbf{P}' . The outputs of **OP3**(\mathcal{Q}, \mathbf{K}') are the optimized s and \mathbf{P} while the outputs of **OP3**(\mathcal{Q}, \mathbf{P}') are the optimized s and \mathbf{K} .

Algorithm 2 Branch and Bound

-
1. Set $\epsilon > 0$ and $k = 0$.
 2. Set $\mathcal{Q}_0 = \mathcal{X}_P \times \mathcal{X}_K$ and $\mathcal{G}_0 = \{\mathcal{Q}_0\}$.
 3. Set $L_0 = \Phi_L(\mathcal{Q}_0)$ and $U_0 = \Phi_U(\mathcal{Q}_0)$.
 4. *while* ($U_k - L_k < \epsilon$)
 5. Select $\bar{\mathcal{Q}}$ from \mathcal{G}_k such that $L_k = \Phi_L(\bar{\mathcal{Q}})$.
 6. Set $\mathcal{G}_{k+1} = \mathcal{G}_k - \{\bar{\mathcal{Q}}\}$.
 7. Split $\bar{\mathcal{Q}}$ along its longest edge into $\bar{\mathcal{Q}}_1$ and $\bar{\mathcal{Q}}_2$.
 8. *for* ($i = 1, 2$)
 9. *if* ($\Phi_L(\bar{\mathcal{Q}}_i) \leq U_k$)
 10. Compute $\Phi_U(\bar{\mathcal{Q}}_i)$.
 11. Set $\mathcal{G}_{k+1} = \mathcal{G}_k \cup \{\bar{\mathcal{Q}}_i\}$.
 12. *end*
 13. *end*
 14. Set $U_{k+1} = \min_{\mathcal{Q} \in \mathcal{G}_{k+1}} \Phi_U(\mathcal{Q})$.
 15. *Pruning* : $\mathcal{G}_{k+1} = \mathcal{G}_{k+1} - \{\mathcal{Q} : \Phi_L(\mathcal{Q}) > U_{k+1}\}$.
 16. Set $L_{k+1} = \min_{\mathcal{Q} \in \mathcal{G}_{k+1}} \Phi_L(\mathcal{Q})$.
 17. Set $k = k + 1$.
 18. *end*
-

Under the various definitions introduced above the *Branch and Bound Algorithm* [32] calculate the global minima of **OP2** to an absolute accuracy of $\epsilon > 0$ within finite time. The pseudocode of *Branch and Bound* method is given in *Algorithm 2*.

APPENDIX C

CONTROL THEORETIC DEFINITIONS AND CONCEPTS

The control theoretic analysis presented in this paper relies on definitions and theorems from three broad areas. These concepts are standard and can be easily found in books like [42], [36].

A. Real Analysis

Definition 1 (Cartesian Product of Sets): Cartesian Products of two sets A and B , denoted by $A \times B$, is defined as the set of all ordered pairs (a, b) where $a \in A$ and $b \in B$.

Notion 1 (Connected Set): A set is said to be connected if for any two points on that set, there exist *at-least* one path joining those two points which also lies on the set. *Note that this is not the "general definition" of connected set.*

Notion 2 (Compact Set): In Euclidian Space \mathbb{R}^n , a closed and bounded set is called a compact set. Also a compact set in \mathbb{R}^n is always closed and bounded. *Note that this is not the "general definition" of compact set.*

B. Linear Algebra

Definition 2 (Euclidian Norm of a Vector): For a vector $x \in \mathbb{R}^n$, euclidian norm $\|x\|$ is defined as $\|x\| := \sqrt{x^T x}$. Throughout the entire paper "norm" means "euclidian norm" unless mentioned otherwise.

Definition 3 (Induced Spectral Norm of a Matrix): For a matrix $A \in \mathbb{R}^{m \times n}$, Induced Spectral Norm $\|A\|$ is defined as

$$\|A\| := \sup_{x \in \mathbb{R}^n - \{0\}} \frac{\|Ax\|}{\|x\|}$$

It can equally be defined as

$$\|A\| := \sup_{\|x\|=1} \|Ax\|$$

Definition 4 (Positive (Negative) Definite (Semi-Definite) Matrix): A square matrix $A \in \mathbb{R}^{n \times n}$ is said to be positive definite if $x^T A x > 0, \forall x \in \mathbb{R}^n - \{0\}$ and is said to be positive semi-definite if $x^T A x \geq 0, \forall x \in \mathbb{R}^n$. A matrix A is said to be negative definite if $-A$ is positive definite and is said to be negative semi-definite if $-A$ is positive semi-definite.

Linear Algebra Theorems:

1) Properties of norms:

- a) For a vector $x \in \mathbb{R}^n$, if $\|x\| = 0$ then $x = 0$. Also if $\|x\| \rightarrow 0$ then $x \rightarrow 0$.
- b) For any two matrix $A, B \in \mathbb{R}^{n \times m}$, $\|A + B\| \leq \|A\| + \|B\|$.
- c) For any matrix $A \in \mathbb{R}^{n \times m}$ and a scalar α , $\|\alpha A\| = \alpha \|A\|$.
- d) For any two matrix $A, B \in \mathbb{R}^{n \times m}$, $\|AB\| \leq \|A\| \|B\|$.
- e) For any matrix $A \in \mathbb{R}^{n \times m}$ and a vector $x \in \mathbb{R}^m$, $\|Ax\| \leq \|A\| \|x\|$.

2) Eigenvalues of symmetric positive (negative) definite matrix are positive (negative).

3) For any symmetric matrix $A \in \mathbb{R}^{n \times n}$ and a vector $x \in \mathbb{R}^n$,

$$\lambda_m(A) \|x\|^2 \leq x^T A x \leq \lambda_M(A) \|x\|^2$$

4) For any symmetric positive definite (semi-definite) matrix A , $\|A\| = \lambda_M(A)$.

5) For any square matrix A , $x^T A x \leq \|A\| \|x\|^2$

C. Convex Analysis

Definition 5 (Convex Set): A set \mathcal{A} is said to be convex if for any $x, y \in \mathcal{A}$, $\theta x + (1 - \theta)y \in \mathcal{A}$, $\forall \theta \in [0, 1]$.

Definition 6 (Convex Function): Let $\mathcal{A} \in \mathbb{R}^n$ be a convex set. A function $f : \mathcal{A} \rightarrow \mathbb{R}$ is convex if

$$f(\theta x + (1 - \theta)y) \leq \theta f(x) + (1 - \theta)f(y)$$

for all $x, y \in \mathcal{A}$ and for all $0 \leq \theta \leq 1$.

Definition 7 (Convex Combination and Convex Hull): Given a set $\mathcal{A} = \{a_1 \ a_2 \ \dots \ a_n\}$, its convex combination are those elements which can be expressed as

$$\theta_1 a_1 + \theta_2 a_2 + \dots + \theta_n a_n$$

where $\theta_1 + \theta_2 + \dots + \theta_n = 1$ and $\theta_i \geq 0, i = 1, 2, \dots, n$.

The set of all convex combination of set \mathcal{A} is called the convex hull of \mathcal{A} . Convex Hull of set \mathcal{A} is indeed the smallest convex set containing \mathcal{A} .

Definition 8 (Semi-Definite Program): A semi-definite program or SDP is an optimization problem in variable $x = [x_1 \ x_2 \ \dots \ x_n]^T \in \mathbb{R}^n$ with the generic structure

$$\begin{aligned} & \text{minimize : } c^T x \\ & \text{subject to :} \\ & F_0 + x_1 F_1 + x_2 F_2 + \dots + x_n F_n \preceq 0 \\ & Ax = b \end{aligned}$$

where $F_0, F_1, F_2, \dots, F_n \in \mathbf{S}$, $c \in \mathbb{R}^n$, $A \in \mathbb{R}^{p \times n}$ and $b \in \mathbb{R}^p$.

ACKNOWLEDGMENT

We would like to thank Prof. Radha Krishna Ganti for providing invaluable help in areas related to convex optimization.

REFERENCES

- [1] L. Chua, "Memristor-the missing circuit element," *IEEE Trans. Circuit Theory*, vol. 18, no. 5, pp. 507–519, 1971.
- [2] D. B. Strukov, G. S. Snider, D. R. Stewart, and R. S. Williams, "The missing memristor found," *Nature*, vol. 453, no. 7191, pp. 80–83, 2008.
- [3] Y. Ho, G. M. Huang, and P. Li, "Dynamical properties and design analysis for nonvolatile memristor memories," *IEEE Trans. Circuits Syst. I, Reg. Papers*, vol. 58, no. 4, pp. 724–736, 2011.
- [4] Y. N. Joglekar and S. J. Wolf, "The elusive memristor: properties of basic electrical circuits," *Eur. J. Phys.*, vol. 30, no. 4, pp. 661–675, 2009.
- [5] F. Corinto and A. Ascoli, "A boundary condition-based approach to the modeling of memristor nanostructures," *IEEE Trans. Circuits Syst. I, Reg. Papers*, vol. 60, pp. 2713–2726, 2012.
- [6] S. Kvatinisky, E. G. Friedman, A. Kolodny, and U. C. Weiser, "Team: Threshold adaptive memristor model," *IEEE Trans. Circuits Syst. I, Reg. Papers*, vol. 60, no. 1, pp. 211–221, 2013.
- [7] S. H. Jo, T. Chang, I. Ebong, B. B. Bhadviya, P. Mazumder, and W. Lu, "Nanoscale memristor device as synapse in neuromorphic systems," *Nano letters*, vol. 10, no. 4, pp. 1297–1301, 2010.
- [8] Y. V. Pershin and M. Di Ventra, "Experimental demonstration of associative memory with memristive neural networks," *Neural Networks*, vol. 23, no. 7, pp. 881–886, 2010.
- [9] A. Sheri, H. Hwang, M. Jeon, and B. Lee, "Neuromorphic character recognition system with two pcmo-memristors as a synapse," *IEEE Trans. Ind. Electron.*, vol. 61, pp. 2933–2941, 2014.
- [10] Y. V. Pershin, S. La Fontaine, and M. Di Ventra, "Memristive model of amoeba learning," *Phys. Rev. E*, vol. 80, no. 2, p. 021926, 2009.
- [11] G. Z. Cohen, Y. V. Pershin, and M. Di Ventra, "Second and higher harmonics generation with memristive systems," *Appl. Phys. Lett.*, vol. 100, no. 13, p. 133109, 2012.
- [12] Y. V. Pershin and M. Di Ventra, "Practical approach to programmable analog circuits with memristors," *IEEE Trans. Circuits Syst. I, Reg. Papers*, vol. 57, no. 8, pp. 1857–1864, 2010.
- [13] S. Shin, K. Kim, and S. Kang, "Memristor applications for programmable analog ics," *IEEE Trans. Nanotechnol.*, vol. 10, no. 2, pp. 266–274, 2011.
- [14] D. Jeltsema and A. Doria-Cerezo, "Port-hamiltonian formulation of systems with memory," *Proc. IEEE*, vol. 100, pp. 1928–1937, 2012.
- [15] D. Jeltsema and A. J. van der Schaft, "Memristive port-hamiltonian systems," *Math. Comput. Model. Dyn. Syst.*, vol. 16, pp. 75–93, 2010.
- [16] J. Hu and J. Wang, "Global uniform asymptotic stability of memristor-based recurrent neural networks with time delays," in *Proc. Int. Joint Conf. Neural Netw.*, 2010, pp. 1–8.
- [17] A. Delgado, "The memristor as controller," in *IEEE Nanotechnology Materials and Devices Conference*, 2010, pp. 376–379.
- [18] J. S. A. Doria-Cerezo, L. van der Heijden, "Memristive port-hamiltonian control: Path-dependent damping injection in control of mechanical systems," in *Proc. 4th IFAC Workshop on Lagrangian and Hamiltonian Methods for Non Linear Control*, 2012, pp. 167–172.
- [19] R. Pasumarthy, G. Saha, F. Kazi, and N. Singh, "Energy and power based perspective of memristive controllers," in *Proc. IEEE Conf. Decis. Contr.*, 2013, pp. 642–647.
- [20] J. J. Gorman and B. Shapiro, *Feedback control of mems to atoms*. Springer, 2011.
- [21] E. Ozalevli and P. E. Hasler, "Tunable highly linear floating-gate cmos resistor using common-mode linearization technique," *IEEE Trans. Circuits Syst. I, Reg. Papers*, vol. 55, pp. 999–1010, 2008.
- [22] L. O. Chua and S. M. Kang, "Memristive devices and systems," *Proc. IEEE*, vol. 64, no. 2, pp. 209–223, 1976.
- [23] T. A. Wey and W. D. Jemison, "Variable gain amplifier circuit using titanium dioxide memristors," *IET Circuits, Devices & Syst.*, vol. 5, no. 1, pp. 59–65, 2011.
- [24] S. Haykin, *Communication systems*, 5th ed. Wiley Publishing, 2009.
- [25] S. P. Boyd, *Linear matrix inequalities in system and control theory*. SIAM, 1994.
- [26] A. Ben-Tal and A. Nemirovski, *Lectures on modern convex optimization: analysis, algorithms, and engineering applications*. SIAM, 2001.
- [27] H. H. Rosenbrock, "The stability of linear time-dependent control systems," *Int. J. Electron. & Contr.*, vol. 15, pp. 73–80, 1963.
- [28] V. Solo, "On the stability of slowly time-varying linear systems," *Math. of Contr., Signals & Syst.*, vol. 7, pp. 331–350, 1994.
- [29] C. B. Barber, D. P. Dobkin, and H. Huhdanpaa, "The quickhull algorithm for convex hulls," *ACM Trans. on Mathematical Software*, vol. 22, no. 4, pp. 469–483, 1996. [Online]. Available: <http://www.qhull.org>
- [30] A. Hassibi, J. How, and S. Boyd, "A path-following method for solving bmi problems in control," in *Proc. Amer. Contr. Conf.*, 1999, pp. 1385–1389.
- [31] Y.-Y. Cao, J. Lam, and Y.-X. Sun, "Static output feedback stabilization: an ilmi approach," *Automatica*, vol. 34, no. 12, pp. 1641–1645, 1998.
- [32] K.-C. Goh, M. Safonov, and G. Papavassilopoulos, "A global optimization approach for the bmi problem," in *Proc. IEEE Conf. Decis. Contr.*, vol. 3, 1994, pp. 2009–2014.
- [33] K. H. H. Fujioaka, "Bounds for the bmi eigenvalue problem - a good lower bound and a cheap upper bound," *Trans. Society of Instr. & Contr. Eng.*, vol. 33, pp. 616–621, 1997.
- [34] M. Michihiro Kawanishi and Y. Shibata, "Bmi global optimization using parallel branch and bound method with a novel branching method," in *Proc. Amer. Contr. Conf.*, 2007, pp. 1664–1669.
- [35] K. Ogata, *Modern Control Engineering*, 5th ed. Prentice Hall, 2010.
- [36] S. Boyd and L. Vandenberghe, *Convex optimization*. Cambridge university press, 2009.
- [37] R. T. Rockafellar, *Convex analysis*. Princeton university press, 1997.
- [38] A. Hassibi, J. How, and S. Boyd, "Low-authority controller design via convex optimization," in *Proc. IEEE Conf. Decis. Contr.*, 1998, pp. 1385–1389.
- [39] I. Barkana, "Simple adaptive control-a stable direct model reference adaptive control methodology-brief survey," *Int. J. Adapt. Contr. Signal Proc.*, 2013.
- [40] I. CVX Research, "CVX: Matlab software for disciplined convex programming, version 2.0," <http://cvxr.com/cvx>, Aug. 2012.
- [41] M. K. Mitsuhiro Fukuda, "Branch-and-cut algorithms for the bilinear matrix inequality eigenvalue problem," *Comput. Optim. Appl.*, vol. 19, p. 2001, 1999.
- [42] E. Kreyszig, *Introductory functional analysis with applications*. Wiley, 1989.



Gourav Saha received the B.E. degree from Anna University, Chennai, India, in 2012. Since 2013, he has been working towards his M.S. (by research) degree in the Department of Electrical Engineering at Indian Institute of Technology, Madras.

His current research interests include application of memristor and memristive systems, control of MEMS and modelling and control of cyber-physical systems with specific focus on cloud computing.



Ramkrishna Pasumarthy obtained his PhD in Systems and Control from the University of Twente, The Netherlands in 2006. He is currently an Assistant Professor at the Department of Electrical Engineering, IIT Madras, India.

His research interests lie in the area of modeling and control of physical systems, infinite dimensional systems and control of computing systems, with specific focus on cloud computing systems.



Prathamesh Khataavkar received the B.Tech degree from University of Pune, India, in 2012. He is currently pursuing his M.S. (by research) degree in the Department of Electrical Engineering at Indian Institute of Technology, Madras.

His current research interests includes Analog/RF IC design.